



LEVEL II



MARCH 1979

LMSC-D676214

AD A088597

INELASTIC RESPONSE OF AN  
INFINITE CYLINDRICAL SHELL  
TO A TRANSIENT ACOUSTIC WAVE

by

T. L. Geers  
C-L. Yen

Sponsored by the Office of Naval Research  
Contract N00014-77-C-0562

Approved for Public Release;  
Distribution Unlimited.

Lockheed Palo Alto Research Laboratory  
Palo Alto, California

DTIC  
ELECTE  
SEP 3 1980  
S D  
D

DDC FILE COPY

80 8 29 011

ABSTRACT

An analytical/computational technique has been developed for determining the geometrically and constitutively nonlinear response of an infinite cylindrical shell to a transverse, transient acoustic wave. Shell behavior has been treated through utilization of the nonlinear structural analyzer DYNAPLAS II, while the fluid-structure interaction has been treated in accordance with both the exact residual potential formulation and the doubly asymptotic approximation. Numerical results produced through application of the approximation differ significantly from the corresponding exact results.

Accession For	
NTIS GRA&I	<input checked="" type="checkbox"/>
DDC TAB	<input type="checkbox"/>
Unannounced	<input type="checkbox"/>
Justification	
By _____	
Distribution/ _____	
Availability Codes	
Dist.	Avail and/or special
A	

DTIC  
ELECTE  
SEP 3 1980  
S D  
D

## FOREWORD

This work was performed under Contract N00014-77-C-0562 with the Office of Naval Research. The authors are grateful to Dr. Nicholas Basdekas of that office for his participation in many fruitful discussions. They are also indebted to Professor Walter Haisler of Texas A & M University for his helpful consultation on the DYNAPLAS Code.

## TABLE OF CONTENTS

<u>Section</u>	<u>Title</u>	<u>Page</u>
1	INTRODUCTION.....	1
2	GOVERNING EQUATIONS.....	3
	2.1 Structural Equations.....	3
	2.2 Fluid-Structure Interaction.....	4
	2.3 Solution Procedure.....	5
3	NUMERICAL RESULTS.....	7
	3.1 Contrived Dry Check Problem.....	7
	3.2 Representative Shock-Wave-Excitation Problem.....	10
	3.3 DAA Response Calculations.....	13
4	CONCLUSION.....	15
5	REFERENCES.....	16
Appendix - REMOVAL OF RIGID-BODY SHELL MOTION.....		35

## LIST OF TABLES AND FIGURES

<u>Table</u>		<u>Page</u>
1	Dry Check Problem Parameters.....	18
2	Dry Check Problem Results.....	18
3	Single-Layer Compromise and Sandwich Shells.....	19

<u>Figure</u>		
1	Geometry of Problem.....	20
2	n=0 Displacement Response of Compromise Shell.....	21
3	n=1 Rigid-Body Displacement Response of Compromise Shell....	22
4	n=2 Flexural Displacement Response of Compromise Shell.....	23
5	n=3 Flexural Displacement Response of Compromise Shell.....	24
6	n=4 Flexural Displacement Response of Compromise Shell.....	25
7	n=5 Flexural Displacement Response of Compromise Shell.....	26
8	Nonaxisymmetric Extensional Displacement Response of Compromise Shell.....	27
9	RPF-DYNA Velocity Response of Compromise Shell.....	28
10	RPF-DYNA Strain Response of Compromise Shell.....	29
11	Deformation Snapshots for the Compromise Shell.....	30
12	n=0 and n=1 Extensional Displacement Response of Compromise Shell as Computed with RPF-DYNA and DAA-DYNA.....	31
13	n=1 and n=2 Flexural Displacement Response of Compromise Shell as Computed with RPF-DYNA and DAA-DYNA.....	32
14	Velocity Response of Compromise Shell as Computed with RPF- DYNA and DAA-DYNA.....	33
15	DAA-DYNA Strain Response of Compromise Shell.....	34

Section 1  
INTRODUCTION

About ten years ago, complete analytical solutions for the two-dimensional, plane-strain response of a linear-elastic, circular cylindrical shell to a transient acoustic wave first appeared [1,2]. The solution techniques involved Fourier decomposition with respect to the circumferential coordinate, followed by the introduction of differential and integral equations to treat the fluid-structure interaction on a harmonic-by-harmonic basis. Recently, these solutions were extended to include geometrically nonlinear behavior of the shell in order to examine the elastic dynamic instability of submerged cylindrical shells [3]. The purpose of the present study has been to extend the solutions still further in order to examine inelastic shell response.

Analytical solutions to idealized problems offer two primary benefits to the technical community. First, they facilitate the development of physical insight into the phenomenology involved. This is not only because of the relative simplicity of the problems treated, but also because of the opportunity to perform extensive parameter studies at modest cost. Second, analytical solutions serve to provide check problems for computer codes developed to treat much more complex problems. Clearly, no code should be applied to complex problems before it is thoroughly tested on a number of check problems.

The present study might not be considered by some to be an analytical study, in that the structural analysis code DYNAPLAS [4,5] is used to treat the geometrically and constitutively nonlinear behavior of the shell. DYNAPLAS was selected for this purpose because it is well established and it is based upon circumferential Fourier decomposition of shell response.

As discussed in Section 2, "live-load" terms have been appended to the DYNAPLAS equations of motion to account for geometrically nonlinear loading effects. These terms, which are derived in [3], are treated as pseudo-forces

during the solution process. Also discussed in Section 2 is the approach selected for treatment of the fluid-structure interaction, viz., the "residual potential formulation" (RPF) of [1]. This approach, which is based upon circumferential Fourier decomposition, constitutes an exact treatment of fluid-structure interaction for a surrounding acoustic medium.

Numerical results are presented in Section 3 for two check problems designed to verify the solution procedure and an inelastic response problem designed to highlight the phenomenology of interest. The response problem involves a shell with elastic/perfectly plastic material behavior that is characterized by a static, elastic, critical-buckling pressure and an axisymmetric elastic-limit pressure that are virtually equal. The shell is excited by a rectangular acoustic wave with a pressure-magnitude equal to four times the shell's elastic critical-buckling pressure and a width equal to four shell radii.

Numerical results are also presented in Section 3 for the inelastic response problem with the fluid-structure interaction treated in accordance with the "doubly asymptotic approximation" (DAA) [6,7]. This approximation, which is the basis for fluid-structure interaction analysis in a number of existing codes [8-13], is asymptotically exact for both low- and high-frequency fluid motions, effecting a smooth transition in the intermediate frequency range. Its computational advantage is that it may be expressed as a matrix ordinary differential equation without requiring discretization of the infinite volume of fluid surrounding the structure.

Section 4 completes the report with a summary of the work performed and a list of conclusions.

Section 2  
GOVERNING EQUATIONS

Consider the two-dimensional, plane-strain motions of the submerged, infinite, circular cylindrical shell of Figure 1. The shell is excited by a transient acoustic wave that first contacts the shell at  $\theta = \pi$ . During the resulting fluid-structure interaction, shell behavior may involve both geometric and constitutive nonlinearity.

2.1 STRUCTURAL EQUATIONS

The decomposition of shell and fluid response into circumferential Fourier harmonics yields

$$\begin{aligned}
 v(\theta, t) &= \sum_{n=1}^{\infty} v_n(t) \sin n\theta \\
 w(\theta, t) &= \sum_{n=0}^{\infty} w_n(t) \cos n\theta \\
 \phi(r, \theta, t) &= \sum_{n=0}^{\infty} \phi_n(r, t) \cos n\theta
 \end{aligned} \tag{1}$$

where  $\phi(r, \theta, t)$  is the velocity potential for the acoustic field. Under such a decomposition, the structural equations of motion for the axisymmetric and  $n$ th nonaxisymmetric response harmonics are [3,4]

$$\begin{aligned}
 \rho_o h \ddot{w}_o + f_o(v, w) &= - [p_o]_{r=a} \\
 \rho_o h \ddot{w}_n + f_{wn}(v, w) &= - [p_n + p_o \left( n \frac{v_n}{a} + \frac{w_n}{a} \right) + \frac{\partial p_o}{\partial r} w_n]_{r=a}, \quad n \geq 1 \\
 \rho_o h \ddot{v}_n + f_{vn}(v, w) &= - [p_o \left( -\frac{v_n}{a} + n \frac{w_n}{a} \right)]_{r=a}, \quad n \geq 1
 \end{aligned} \tag{2}$$

where  $p_n(r,t)$  is the  $n$ th harmonic of fluid pressure and  $f_0$ ,  $f_{wn}$  and  $f_{vn}$  are stiffness-force harmonics computed within DYNAPLAS that involve linear-elastic, geometrically nonlinear and constitutively nonlinear behavior.

The terms on the right sides of (2) that involve pressure-displacement products are "live-load" terms appropriate to moderate displacements and rotations of the shell surface. They account for the major effect of finite membrane strain and finite rotation of shell normals on shell excitation by a normal pressure loading, as well as the primary effect of finite shell displacement on the loading produced by the spatially varying acoustic field [3]. Without these terms, the right sides of (2) would involve only "dead load" terms appropriate to infinitesimal shell motions. As DYNAPLAS does not possess live-load capability, the live-load terms have been treated as pseudo-forces generated by auxiliary software.

## 2.2 FLUID STRUCTURE INTERACTION

A residual potential formulation (RPF) of the fluid-structure interaction, which constitutes an exact treatment, may be constructed as follows [1]. First, fluid pressure and radial fluid-particle velocity are expressed as derivatives of the fluid velocity potential as

$$\begin{aligned} p &= -\rho \dot{\phi} \\ u &= \partial \phi / \partial r \end{aligned} \tag{3}$$

Second, the total acoustic field is treated as the superposition of the acoustic field for the known incident wave and the acoustic field for the unknown scattered wave, i.e.,

$$\phi(r,\theta,t) = \phi_I(r,\theta,t) + \phi_S(r,\theta,t) \tag{4}$$

Third, compatibility of radial fluid-particle velocity and radial shell velocity is enforced at the wet surface of the shell as

$$u(a, \theta, t) = \dot{w}(\theta, t) \quad (5)$$

Finally, the wave equation and radiation condition for each circumferential harmonic of the scattered wave are replaced by the equivalent residual-potential equation

$$\frac{\partial \phi_{Sn}}{\partial r} + \frac{1}{c} \dot{\phi}_{Sn} + \frac{1}{2r} \phi_{Sn} = \frac{1}{r} \phi_{Rn} \quad (6)$$

in which the residual potential  $\phi_{Rn}$  is given by the convolution relation

$$\phi_{Rn}(r, t) = - \int_0^t r_n(r, t') \phi_{Sn}(r, t-t') dt \quad (7)$$

where the  $r_n$  are characteristic functions that resemble step-exponential functions [1].

Equations (3) - (7) may be utilized to produce, for each circumferential harmonic, the fluid-structure-interaction relations

$$p_n^a = - \rho (\dot{\phi}_{In}^a + \dot{\phi}_{Sn}^a)$$

$$\frac{\partial p_o^a}{\partial r} = - \rho \ddot{w}_o \quad (8)$$

$$\dot{w}_n + \frac{1}{c} \dot{\phi}_{Sn}^a + \frac{1}{2a} \phi_{Sn}^a = u_{In}^a + \frac{1}{a} \phi_{Rn}^a$$

where  $\phi_{Rn}^a = \phi_{Rn}(a, t)$  is obtained from (7).

### 2.3 SOLUTION PROCEDURE

In principle, (2), (7) and (8) may be solved simultaneously in direct fashion for a selected number of Fourier harmonics; Fourier superposition in accordance with (1) then produces response histories of interest. In prac-

tice, however, care must be taken to provide an implementation that yields solutions of satisfactory accuracy at acceptable computational cost. As verified in Section 3, such an implementation has been constructed in non-dimensional form in accordance with the normalization

$$\hat{p} = p^a/\rho c^2, \quad \hat{w} = w/a, \quad \hat{t} = ct/a \quad (9)$$

The nondimensional response equations underlying the implementation used for computations are [cf. (2), (7) and (8)]

$$\begin{aligned} \left(\frac{\rho}{\rho_0}\right) \left(\frac{h}{a}\right) \ddot{w}_0 + \dot{w}_0 + f_0(v,w) &= \dot{\phi}_{I0} + u_{I0} - \frac{1}{2} \phi_{S0} + \phi_{R0} \\ \left(\frac{\rho}{\rho_0}\right) \left(\frac{h}{a}\right) \ddot{w}_n + \dot{w}_n + f_{wn}(v,w) &= \dot{\phi}_{In} + u_{In} - \frac{1}{2} \phi_{Sn} + \phi_{Rn} \\ &+ (\dot{\phi}_{I0} + \dot{\phi}_{S0})(nv_n + w_n) + \ddot{w}_0 w_n, \quad n \geq 1 \\ \left(\frac{\rho}{\rho_0}\right) \left(\frac{h}{a}\right) \ddot{v}_n + f_{vn}(v,w) &= (\dot{\phi}_{I0} + \dot{\phi}_{S0})(v_n + nw_n), \quad n \geq 1 \\ \dot{\phi}_{Sn} + \frac{1}{2} \phi_{Sn} &= u_{In} - \dot{w}_n + \phi_{Rn} \\ \phi_{Rn} &= -r_n * \phi_{Sn} \end{aligned} \quad (10)$$

where all circumflexes have been dropped,  $\dot{w}_0 \equiv d\hat{w}_0/d\hat{t}$ , etc., and the asterisk denotes temporal convolution, as defined in (7). For  $n = 0$ , (10) contains three equations for the three unknowns  $w_0$ ,  $\phi_{S0}$  and  $\phi_{R0}$ , while for each  $n \geq 1$ , (10) contains four equations for the four unknowns  $w_n$ ,  $v_n$ ,  $\phi_{Sn}$  and  $\phi_{Rn}$ . From a computational standpoint, the primary advantage of (10) is that the terms involving unknowns on the right sides of the first three of (10) are more slowly varying than the acceleration and velocity terms on the left sides.

The combined response equations (10) were solved by step-by-step numerical integration as follows. The first three of (10) were solved with the half-step central-difference algorithm [14], which was introduced into DYNAPLAS for reasons given in Section 3. This modification also involved the introduction of structural damping analysis capability into DYNAPLAS to treat the velocity terms on the left sides of the first two of (10). The fourth of (10) was solved with a fourth-order Runge-Kutta scheme [15], as in [3]. Finally, the last of (10) was solved with trapezoidal integration, as in [3]. This procedure possessed satisfactory accuracy, stability and efficiency characteristics.

### Section 3 NUMERICAL RESULTS

As seen in Section 2, the derivation of the structural and fluid-structure-interaction equations in accordance with [3] and [4] is relatively straightforward. The establishment of a satisfactory solution procedure, which involves the interfacing of two distinct computer codes, is not straightforward. Presented in this section are numerical results for two check problems designed to verify the solution procedure and a response problem representative of the phenomenology of interest, viz., the geometrically and constitutively nonlinear behavior of shock-wave-excited, submerged shells. All results are presented in nondimensional form normalized in accordance with (9).

#### 3.1 CONTRIVED DRY CHECK PROBLEM

Consider an infinite elastic, circular cylindrical shell responding in plane strain to the prescribed surface pressure loading

$$p(\theta, t) = -P_0 \frac{t}{t_0} H(t) H(t_0 - t) - P_0 H(t - t_0) \quad (11)$$
$$-P_n \frac{t - t_1}{t_n} H(t - t_1) \cos n\theta, \quad n \geq 2$$

where  $H(t)$  is the Heaviside step-function. For  $t_1 > t_0$ , (11) constitutes an axisymmetric ramp-step loading followed by a nonaxisymmetric ramp loading of specified harmonic index. If  $t_1 \gg t_0$  and an axisymmetric damping mechanism is present (which is the situation considered here), axisymmetric shell response reaches its static asymptote before the nonaxisymmetric loading is applied. Subsequent nonaxisymmetric shell response then constitutes that of a hydrostatically pressurized shell.

As discussed in [3], nonaxisymmetric shell response to (11) is essentially inextensional. Hence, for  $t_1 \gg t_0$  and appreciable damping of axisymmetric shell response, nonaxisymmetric response to (11) is governed by the equation [3]

$$m_n \ddot{w}_n + m_n \omega_n^2 w_n = -P_n \frac{t-t_1}{t_n} H(t-t_1) \quad (12)$$

in which

$$m_n = \left(\frac{\rho_o}{\rho}\right) \left(\frac{h}{a}\right) \frac{n^2+1}{n^2} \quad (13)$$

$$\omega_n = \frac{1}{\sqrt{12}} \left(\frac{c_o}{c}\right) \left(\frac{h}{a}\right) \left(\frac{n^2}{n^2+1}\right)^{1/2} (n^2-1) (1-P_o/P_{cn})^{1/2}$$

where  $c_o = [E_o/\rho_o(1-\nu_o^2)]^{1/2}$  is the plate velocity of the shell material and  $P_{cn} = (n^2-1)(\rho_o/\rho)(c_o/c)^2(h^3/12a^3)$  is the static critical buckling pressure for the nth circumferential harmonic. The solution to (12) for quiescent initial conditions is

$$w_n = S_n \left(t-t_1 - \frac{T_n}{2\pi} \sin 2\pi \frac{t-t_1}{T_n}\right) H(t-t_1) \quad (14)$$

where the response slope  $S_n$  and the natural period  $T_n$  are given by

$$S_n = \frac{P_n}{m_n \omega_n^2 t_n} \quad (15)$$

$$T_n = \frac{2\pi}{\omega_n}$$

DYNAPLAS II and DYNAPLAS III computations were performed for  $n = 2-5$  on the basis of (2) and (11) with  $\partial p_o/\partial r = 0$ ; the parameter values chosen for the computations are shown in Table 1. The Houbolt time-integration scheme was used, which is characterized by high algorithmic damping for time-increment/natural-period ratios greater than 0.1 [16]. Hence, with the time increments of Table 2 constituting one-half or one-quarter of the period of the  $n = 0$  shell mode, hydrostatic conditions were reached well before application of the nonaxisymmetric loading in every calculation.

The response-slope and natural-period values gleaned from the response computations are shown in Table 2. Good agreement is observed between the

DYNAPLAS II and analytical values. The discrepancies that exist are primarily due to the relatively poor accuracy characteristics of the Houbolt scheme [16]. Appreciable discrepancies exist between the DYNAPLAS III and analytical values for  $n = 2$ , however. Furthermore, no DYNAPLAS III values are shown for  $n \geq 3$ , because, for these harmonics, the code erroneously produced nonaxisymmetric response results for  $t < t_1$ , when only the axisymmetric loading was present.

It should be mentioned that a "dead-load" version of Table 2 was also compiled, corresponding to neglect to the pressure-displacement products on the right sides of (2). This was done to ensure that no discrepancy between a DYNAPLAS result and an analytical result could be attributed to the auxiliary live-load software mentioned in Subsection 2.1. The dead-load discrepancies observed were entirely consistent with those of Table 2.

In view of Table 2, DYNAPLAS II was selected as the structural analyzer for the present study. This was originally somewhat of a disappointment, because DYNAPLAS II does not treat multilayer shells, whereas DYNAPLAS III does. Multilayer analysis capability was desired in order to use a sandwich shell as a plane-strain model for a stiffened shell, as discussed in [1]. This modeling problem was satisfactorily overcome, however, as described below.

Because of the rather severe accuracy limitations of the Houbolt scheme, the half-step central-difference scheme [14] was introduced into DYNAPLAS II to integrate the augmented structural response equations given by the first three of (10). This produced much better accuracy relative to elastic-shell results presented in [3] than that provided by the whole-step central-difference scheme already existing in DYNAPLAS II. Hence accuracy requirements, which mandated augmentation of the structural response equations, also mandated restructuring of the DYNAPLAS II integrator.

Finally, one additional note regarding DYNAPLAS calculation should be mentioned. It was found that the default operation involving static condensation of the rigid-body shape-function coefficients (the  $\beta$ 's of p 24 in [4]) produced an erroneous linear stiffness matrix for  $n = 1$ . The entry of "1" in Column 30 of Card 3 in the SAMSØR4 input deck overrides the default operation, thereby correcting the problem.

### 3.2 REPRESENTATIVE SHOCK-WAVE-EXCITATION PROBLEM

Consider a submerged, infinite, circular cylindrical shell responding in plane strain to an incident wave of rectangular pressure-profile. The desired shell would be a sandwich shell, exhibiting the enhanced flexural stiffness properties characteristic of stiffened shells [1]. Because DYNAPLAS II is limited to the treatment of single-layer shells, however, a compromise shell is considered. As outlined in Table 3, the single-layer compromise shell possesses inertial and elastic properties, and static-elastic-stability and extensional elastic-limit characteristics that are identical to those for a sandwich shell with properties representative of a stiffened steel shell. The two shells differ somewhat with respect to their inelastic flexural characteristics, however.

Figures 2-15 show response results pertaining to excitation of the compromise shell by a transverse plane wave of rectangular pressure-profile that first contacts the shell at  $\theta = \pi$  (Figure 1). The magnitude of the incident wave,  $P_I$ , is equal to four times the shell's elastic critical-buckling pressure,  $P_C$ , which is, in turn, nearly equal to the shell's axisymmetric elastic-limit pressure,  $P_0$ . The width of the rectangular wave is four shell radii ( $T_I = 4$ ): the incident wave loading is of moderately long duration. The  $n = 0-5$  circumferential harmonics are considered and the nonlinear material behavior of the shell is taken as elastic/perfectly plastic.

Shown along with inelastic results are results pertaining to nonlinear elastic shell response, as calculated by the present code RPF-DYNA and the small dynamic buckling program RPF-DBP [3]. (Good agreement between the RPF-DYNA and RPF-DBP results has been a verification requirement for the RPF-DYNA software.) Also shown for comparison purposes are linear-elastic results. Finally, it is important to remember that all displacement and velocity histories are normalized to the magnitude of the incident rectangular wave,  $P_I$ , which is  $9.62 \times 10^{-3}$  on a nondimensional basis; on a dimensional basis, it is this value times  $\rho c^2$ .

Figure 2 shows  $n = 0$  displacement histories with inelastic shell behavior both included and excluded. It is seen that the nonlinear-elastic (N-E) RPF-DYNA and RPF-DBP histories are coincident with the linear-elastic (L-E) RPF-DYNA history. When inelastic shell behavior is included,  $n = 0$  response grows rapidly after the  $n = 0$  elastic-limit displacement  $w_{o\ell} = -0.27 P_I = -0.0026$  is reached; the motion slows, however, as the incident wave passes beyond the shell, leaving an  $n = 0$  set displacement of  $w_{os} = -6.87 P_I = -0.0661$ . Note the absence of oscillatory behavior in all the  $n = 0$  response histories; this is the result of the heavy acoustic damping provided by the surrounding fluid [1,2].

In [3], the radial and circumferential displacement harmonics  $w_n$  and  $v_n$ ,  $n \geq 1$ , are expressed in terms of the extensional and flexural displacement harmonics  $e_n$  and  $f_n$  as

$$\begin{aligned} v_n &= n e_n - \frac{1}{n} f_n \\ w_n &= e_n + f_n \end{aligned} \tag{16}$$

Consideration of the  $e_n$  and  $f_n$  provides greater insight into the physical processes at work than does consideration of  $v_n$  and  $w_n$ ; hence  $e_n$  and  $f_n$  histories are shown here.

Figure 3 shows  $n = 1$  flexural displacement histories, which constitute rigid-body motion, for both elastic and inelastic shell response. The coincident nonlinear-elastic RPF-DYNA and RPF-DBP histories follow closely the linear-elastic RPF-DYNA history, while the inelastic RPF-DYNA history deviates significantly from the elastic histories. This deviation is caused by greatly increased  $n = 1$  extensional response (as discussed later), which feeds back through the fluid-structure interaction to affect rigid-body motion [see the last of (8) and the last of (16)]. The small late-time velocities exhibited by the nonlinear response histories are due to the pressure-gradient term in the second of (2). When this term is omitted, the nonlinear-elastic histories coincide with the linear-elastic history and the nonlinear-inelastic history approaches an asymptotic displacement of  $f_1/P_I = 8.0$ . Small effects of the pressure-gradient term are also found in the  $n \geq 2$  response histories.

Appreciable differences among linear-elastic, nonlinear-elastic, and inelastic histories are exhibited in Figure 4, which shows  $n = 2$  flexural displacement response. A small discrepancy between the nonlinear-elastic RPF-DYNA and RPF-DBP histories also appears at late times. For  $t \gtrsim 7$ , inelastic  $f_2$ -response consists of lightly damped oscillations about a set displacement whose value cannot be discerned from the figure.

Figure 5 shows  $n = 3$  flexural displacement histories for the shell. The nonlinear-elastic RPF-DYNA and RPF-DBP histories are in satisfactory agreement, with the linear-elastic and inelastic response histories of comparable magnitude but differing phase. As stated earlier, the response calculations included the  $n = 4$  and  $n = 5$  harmonics; flexural displacement histories for these are presented in Figures 6 and 7. The figures show elastic-response histories that, in view of their magnitudes, differ unimportantly from one another, and inelastic-response histories that oscillate at late times about modest set displacements.

For elastic shell behavior, it shown in [3] that nonaxisymmetric extensional response is negligible, and the  $e_n$  may be ignored. For inelastic shell motion, this is not the case, as shown in Figure 8. The figure shows extensional displacement histories for  $n = 1-5$  inelastic shell response, as well as for  $n = 1$  nonlinear-elastic shell response; nonlinear-elastic shell response for  $n \geq 2$  would be barely visible in this figure.

Figure 9 shows radial-velocity histories at  $\theta = 0$  and  $\theta = \pi$  for inelastic, nonlinear-elastic and linear-elastic response. It is seen that the nonlinear-elastic histories differ little from their linear-elastic counterparts, but that the inelastic histories deviate substantially from their elastic counterparts.

It is in the strain histories of Figure 10 that the substantial  $n = 1$  and 2 extensional responses observed in Figure 8 clearly manifest themselves. They are responsible for the largest set strains occurring on the back side

of the shell, with the maximum occurring at  $\theta = 0$ . The proximity of the inner-fiber and outer-fiber strain histories for each  $\theta$ -location illustrate the relative unimportance of flexural strain in the compromise shell. Such strain would be even less important in the corresponding sandwich shell with its smaller total thickness.

Finally, Figure 11 shows deformation snapshots at  $t = 5, 10, 15,$  and  $20$  for inelastic, nonlinear-elastic and linear-elastic shell response. These are obtained by the simple removal of rigid-body shell motion during Fourier synthesis, which yields (see Appendix)

$$v_d(\theta, t) = \frac{1}{2}[v_1(t) + w_1(t)] \sin\theta + \sum_{n=2}^{\infty} v_n(t) \sin n\theta \quad (17)$$

$$w_d(\theta, t) = w_0(t) + \frac{1}{2}[v_1(t) + w_1(t)] \cos\theta + \sum_{n=2}^{\infty} w_n(t) \cos n\theta$$

The inelastic-response snapshots exhibit large axisymmetric deformation; the modest nonaxisymmetric contribution is such that maximum deformation appears at  $\theta = 0$  when  $t = 10, 15$  and  $20$ . In comparison, the elastic-response snapshots exhibit appreciably smaller deformations dominated by  $f_2$ -displacement.

### 3.3 DAA RESPONSE CALCULATIONS

One of the purposes of the present study has been to examine the accuracy of inelastic transient-response solutions based upon approximate treatment of the fluid-structure interaction in accordance with the doubly asymptotic approximation (DAA) [6,7]. To this end, Figures 12-15 show RPF-DYNA and DAA-DYNA inelastic-response histories for the shock-wave-excitation problem considered in the previous subsection.

Figure 12 shows  $n = 0$  and  $n = 1$  extensional displacement histories for the rectangular-wave-excited cylindrical shell. Large discrepancies between the DAA histories and their RPF counterparts are seen, with the DAA seriously

underestimating shell response. Note that the late-time asymptote for DAA  $n=1$  response is of opposite sign with respect to its RPF counterpart. The impact of this difference on strain response will be seen shortly. Large discrepancies between DAA-based and RPF-based flexural displacement histories for  $n=1$  and 2 are seen in Figure 13. While these discrepancies have little or no effect in strain response comparisons, they play a substantial role in kinematic response comparisons. Radial velocity histories at  $\theta=0$  and  $\theta=\pi$  are shown in Figure 14. The DAA-inelastic histories are seen to lie somewhere between their RPF-inelastic and RPF-elastic counterparts, the latter appearing in Figure 9. Hence the DAA calculations tend to underestimate velocity-response magnitudes on the side of the shell facing the incident wave, and to overestimate them on the back side of the shell.

Finally, Figure 15 shows DAA-computed strain histories at  $\theta=0$ ,  $\pi/2$  and  $\pi$ . A comparison of these histories with their RPF-computed counterparts in Figure 10 is rather startling. Not only is peak strain underestimated by a factor of 2.4, but the location of peak strain occurrence is completely missed, the DAA-calculations placing it at  $\theta=\pi$  and the RPF-calculations placing it at  $\theta=0$ . This is the direct result of the sign difference in the DAA and RPF late-time asymptotes for  $n=1$  extensional displacement response (see Figure 12).

Figures 12-15 clearly exhibit failure of the DAA as an accurate method for treatment of the fluid-structure interaction in the present problem. The reason for this failure may be stated briefly as follows. The strain field in the shell is dominated by the  $n=0$  harmonic. But the DAA, for  $n=0$  motion of an infinite, circular cylindrical body, is no longer doubly asymptotic, because the added mass for such motion is infinite [17]. Hence the DAA reduces to the plane wave approximation, which seriously attenuates the response.

Section 4  
CONCLUSION

This study has involved the formulation, implementation, and execution of an analytical/computational technique for determining the geometrically and constitutively nonlinear response of an infinite cylindrical shell to a transverse, transient acoustic wave. The fluid-structure interaction has been treated in accordance with both the exact residual potential formulation and the doubly asymptotic approximation. Shell behavior has been treated through utilization of the nonlinear structural analyzer DYNAPLAS II.

During the study, the following conclusions have been drawn:

1. The formulation and implementation described in Section 2 are accurate and efficient.
2. DYNAPLAS II is a suitable structural analyzer for problems of this type, even though it is limited to the treatment of single-layer shells; DYNAPLAS III is not suitable.
3. For the particular shock-wave-excitation problem considered, axisymmetric shell response plays the dominant role regarding inelastic shell behavior.
4. In spite of the dominance of axisymmetric response, nonaxisymmetric extensional response emerges as an important contributor to shell deformation; this is in contrast to the case of elastic shell behavior, where such response is negligible.
5. The set profile produced in the particular shock-wave-excitation problem considered resembles an oval, with the largest set strains occurring on the back side of the shell.
6. In the particular shock-wave-excitation problem considered, the DAA fails as an accurate method for treatment of the fluid-structure interaction.
7. Further studies are needed to provide a broader assessment of the suitability of the DAA for this class of problems.

Section 5  
REFERENCES

1. T. L. Geers, "Excitation of an Elastic Cylindrical Shell by a Transient Acoustic Wave", J. Appl. Mech., 36, 459-469, September 1969.
2. H. Huang, "An Exact Analysis of the Transient Interaction of Acoustic Plane Waves with a Cylindrical Elastic Shell", J. Appl. Mech., 37, 1091-1106, December 1970.
3. T. L. Geers and C.-L. Yen, "Dynamic Instability of an Elastic Cylindrical Shell Excited by a Transient Acoustic Wave", DNA 5026Z, Defense Nuclear Agency, Washington, D.C., July 1979.
4. W. E. Haisler, J. A. Stricklin and W. A. Von Rieseemann, "DYNAPLAS--A Finite Element Program for the Dynamic, Large Deflection, Elastic-Plastic Analysis of Stiffened Shells of Revolution", Rpt. No. TEES-RPT-72-27, Texas A&M University, College Station, TX, December 1972.
5. W. E. Haisler, personal communication; DYNAPLAS III is an updated version of DYNAPLAS II that has never been officially released, but has been distributed informally to some users.
6. T. L. Geers, "Residual Potential and Approximate Methods for Three-Dimensional Fluid-Structure Interaction Problems", J. Acoust. Soc. Am., 49, 1505-1510, May 1971.
7. T. L. Geers, "Doubly Asymptotic Approximations for Transient Motions of Submerged Structures", J. Acoust. Soc. Am., 64, 1500-1508, November 1978.
8. G. C. Everstine, "A NASTRAN Implementation of the Doubly Asymptotic Approximation for Underwater Shock Response", NASTRAN: Users Experiences, NASA TM X-3428, 207-228, October 1976.
9. D. Ranlet, F. L. DiMaggio, H. H. Bleich and M. L. Baron, "Elastic Response of Submerged Shells with Internally Attached Structures to Shock Loading", Composites and Structures, 7, 355-364, June 1977.
10. J. A. DeRuntz, T. L. Geers, and C. A. Felippa, "The Underwater Shock Analysis (USA) Code, A Reference Manual", DNA Report 4524F, Defense Nuclear Agency, Washington, D.C., February 1978.
11. J. A. DeRuntz and F. A. Brogan, "Underwater Shock Analysis of Nonlinear Structures, A Reference Manual for the USA-STAGS Code", LMSC-D624355, Lockheed Palo Alto Research Laboratory, Palo Alto, CA, February 1978.
12. J. E. Roderick, R. F. Jones, and M. G. Costello, "TRAINS - A Finite Element Computer Program for the Transient, Large Deflection Analysis of Inelastic Structures", Report M-17, David W. Taylor Naval Ship R&D Center, Bethesda, MD, February 1978.

13. R. Atkatch, M. P. Bieniek and M. L. Baron, "Dynamic Elasto-Plastic Response of Shells in an Acoustic Medium - Theoretical Development for the EPSA Code", Tech. Rpt. No. 24, Weidlinger Assoc., Consulting Engineers, New York, NY, July 1978.
14. G. Dahlquist and Å. Björk, Numerical Methods, Prentice-Hall, Inc., Englewood Cliffs, NJ, 1974, p. 353.
15. L. Lapidus and J. H. Seinfeld, Numerical Solution of Ordinary Differential Equations, Academic Press, NY, 1971, p. 50.
16. K. C. Park, "Evaluating Time Integration Methods for Nonlinear Dynamics Analysis", 35-48 of Finite Element Analysis of Transient Nonlinear Structural Behavior, AMD Vol. 14, ASME, New York, NY, 1975.
17. T. L. Geers, "Shock Response Analysis of Submerged Structures", Shock and Vibration Bulletin, 44 (3), 17-32, August 1974

Table 1. DRY CHECK PROBLEM PARAMETERS

Shell of Figure 1:  $\rho_o g = 596$ ,  $E_o = 17.5068$ ,  $\nu_o = 0.3$ ,  $h = 0.05$ ,  $a = 1$

Loading of Eq. (11):  $P_o = \frac{3}{4} P_{cn} = 1.503 \times 10^{-4} (n^2 - 1)$

$P_n = 10^{-3} P_{cn} = 2.004 \times 10^{-7} (n^2 - 1)$

$t_o = 8.9$ ,  $t_1 = 44.5$ ,  $t_n = 2T_n$

$g = 386$ ;  $P_{cn}$  defined after (13);  $T_n$  given by (13) and (15)

Calculations performed for  $0 \leq t \leq t_1 + t_n$

The shell parameters shown pertain to a steel sandwich shell with flexural stiffness "EI" twenty-five times that of a monocoque steel shell with  $h/a = 0.01$  (see Table 3 for equivalence technique).

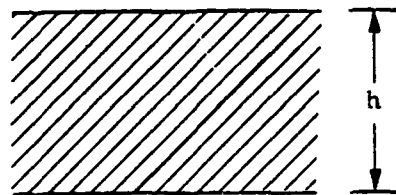
Table 2. DRY CHECK PROBLEM RESULTS

$(T_n/S_n \times 10^6)$

<u>n</u>	<u><math>\Delta t</math></u>	<u>From (15)</u>	<u>DYNAPLAS II</u>	<u>DYNAPLAS III</u>
2	0.89	91.9/7.25	92.6/7.26	57.9/2.80
3	0.89	32.5/7.69	33.8/7.69	
4	0.445	16.9/7.87	17.8/7.67	
5	0.445	10.5/7.95	11.7/7.78	

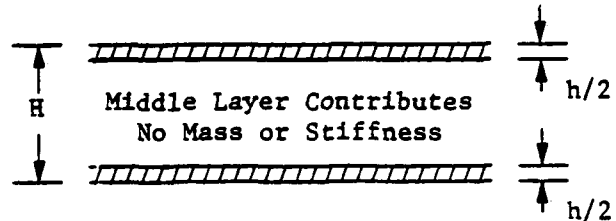
Table 3. SINGLE-LAYER COMPROMISE AND SANDWICH SHELLS \*

Single-Layer Shell



$$\frac{h}{a} = 0.1$$

Sandwich Shell



$$\frac{h}{a} = 0.01, \quad \frac{H}{a} = 0.06266$$

$$\frac{\rho_o}{\rho} = 0.772, \quad \frac{c_o}{c} = 3.53, \quad \frac{\sigma_y}{\rho c^2} = 0.02188 \quad \frac{\rho_o}{\rho} = 7.72, \quad \frac{c_o}{c} = 3.53, \quad \frac{\sigma_y}{\rho c^2} = 0.2188$$

Inertial and Elastic Properties

$$" \rho c " = \frac{\rho_o h}{\rho a} = 0.0772, \quad " Et " = \frac{\rho_o c_o^2 h}{\rho c^2 a} = 0.9620 \quad " \rho c " = \frac{\rho_o h}{\rho a} = 0.0772, \quad " Et " = \frac{\rho_o c_o^2 h}{\rho c^2 a} = 0.9620$$

$$" EI " = \frac{\rho_o c_o^2}{\rho c^2} \cdot \frac{1}{12} \left( \frac{h}{a} \right)^3 = 8.017 \times 10^{-4} \quad " EI " = \frac{\rho_o c_o^2}{\rho c^2} \cdot \frac{100}{12} \left( \frac{h}{a} \right)^3 = 8.017 \times 10^{-4}$$

Static-Elastic-Stability and Extensional Elastic-Limit Characteristics

$$P_c = \frac{1}{2} \left( \frac{\rho_o}{\rho} \right) \left( \frac{c_o}{c} \right)^2 \left( \frac{h}{a} \right)^3 = 2.405 \times 10^{-3} \quad P_c = 25 \left( \frac{\rho_o}{\rho} \right) \left( \frac{c_o}{c} \right)^2 \left( \frac{h}{a} \right)^3 = 2.405 \times 10^{-3}$$

$$N_y = \left( \frac{h}{a} \right) \left( \frac{\sigma_y}{\rho c^2} \right) = 2.462 \times 10^{-3} \quad ** \quad N_y = \left( \frac{h}{a} \right) \left( \frac{\sigma_y}{\rho c^2} \right) = 2.462 \times 10^{-3} \quad **$$

Inelastic Flexural Characteristics

$$M_y = 4.103 \times 10^{-5}$$

$$K_y = 0.05118$$

$$M_u = 6.155 \times 10^{-5}$$

Yield Moment  
Yield Curvature  
Ultimate Moment

$$M_y = 6.549 \times 10^{-5}$$

$$K_y = 0.08170$$

$$M_u = 7.099 \times 10^{-5}$$

\* See Figure 1 for parameter definitions

\*\* von Mises yield condition with  $\nu = 0.3$

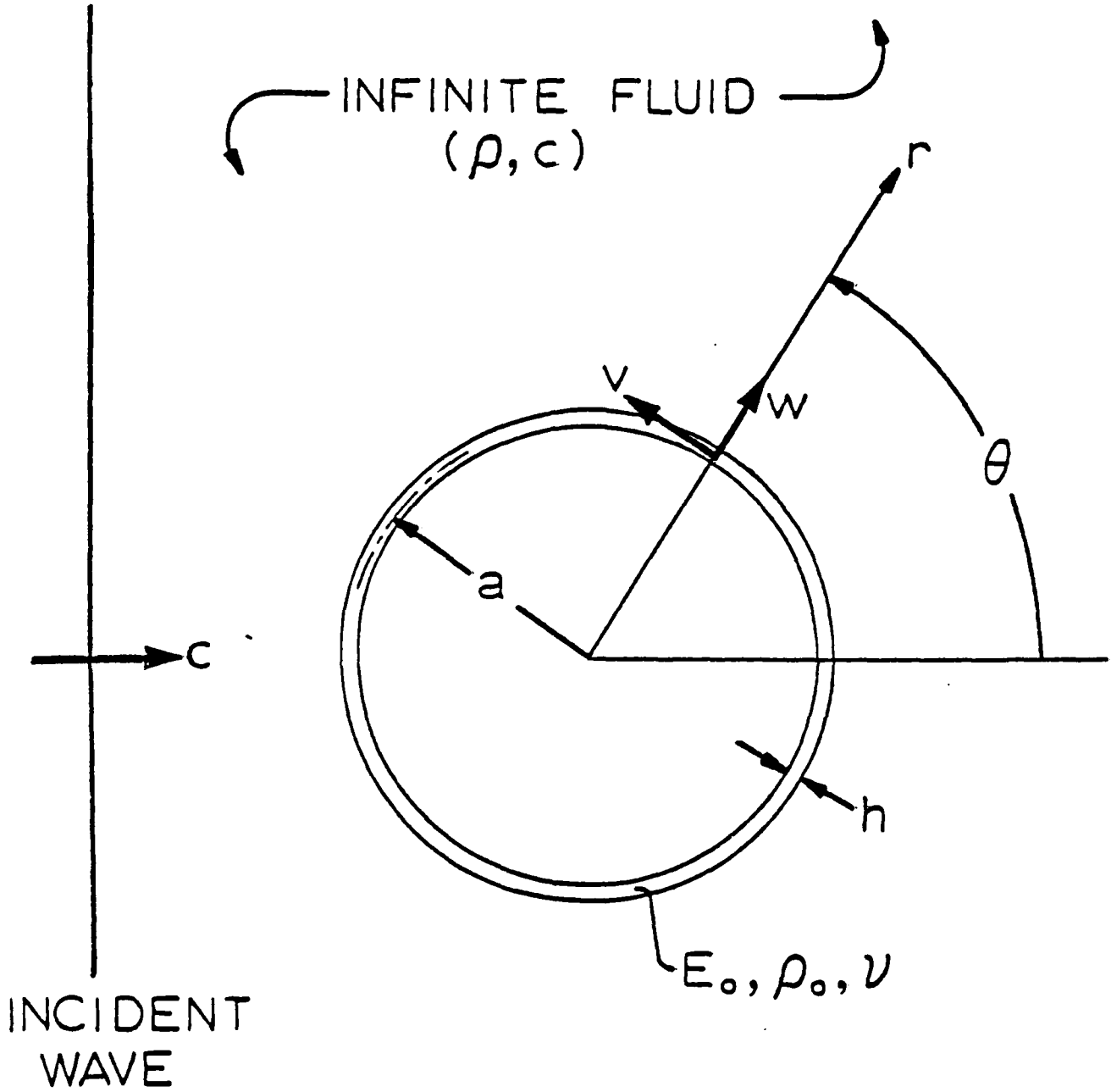


Figure 1. Geometry of Problem

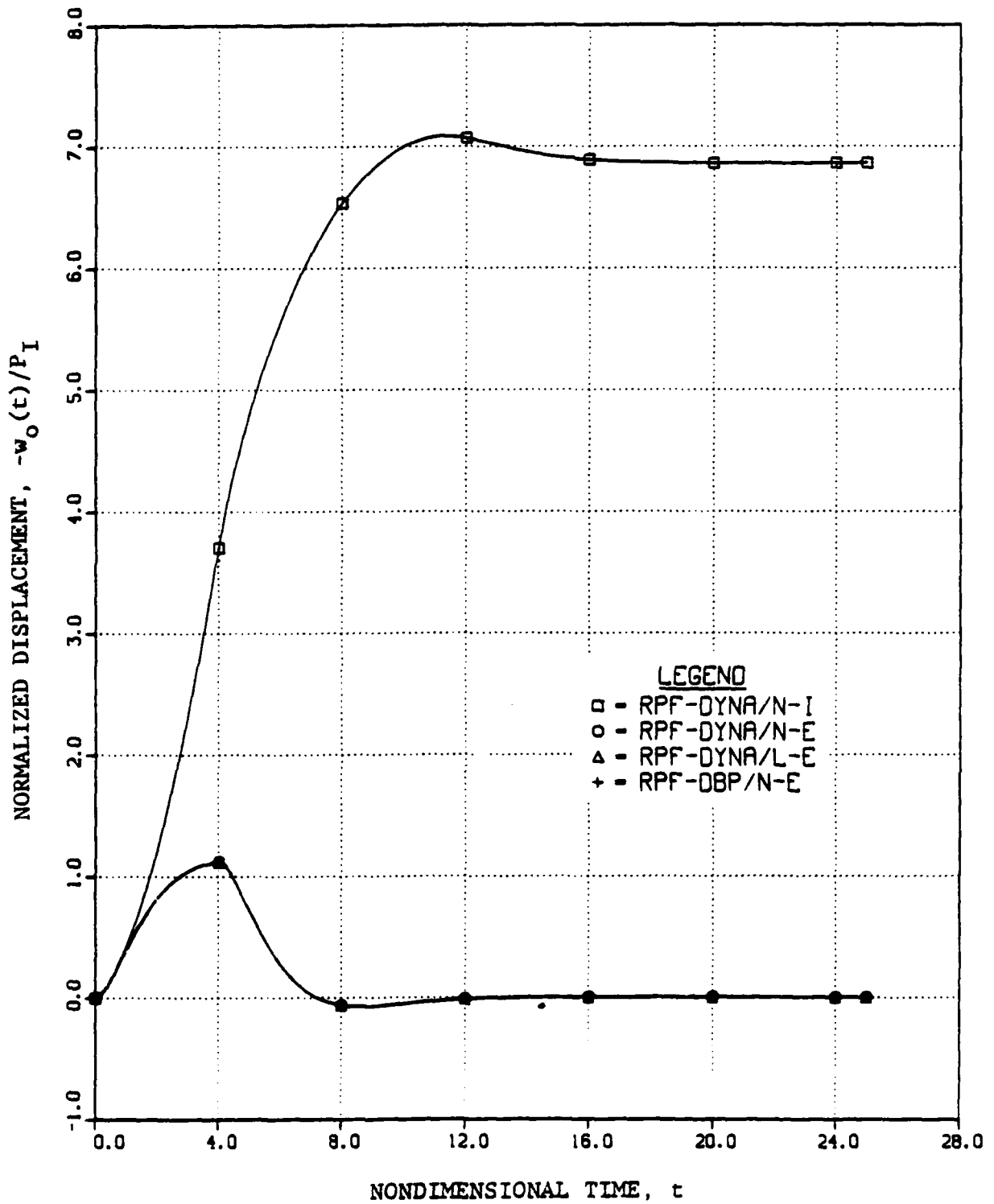


Figure 2.  $n=0$  Displacement Response of Compromise Shell  
 $(P_I = 4P_c \approx 4P_0, T_I = 4)$

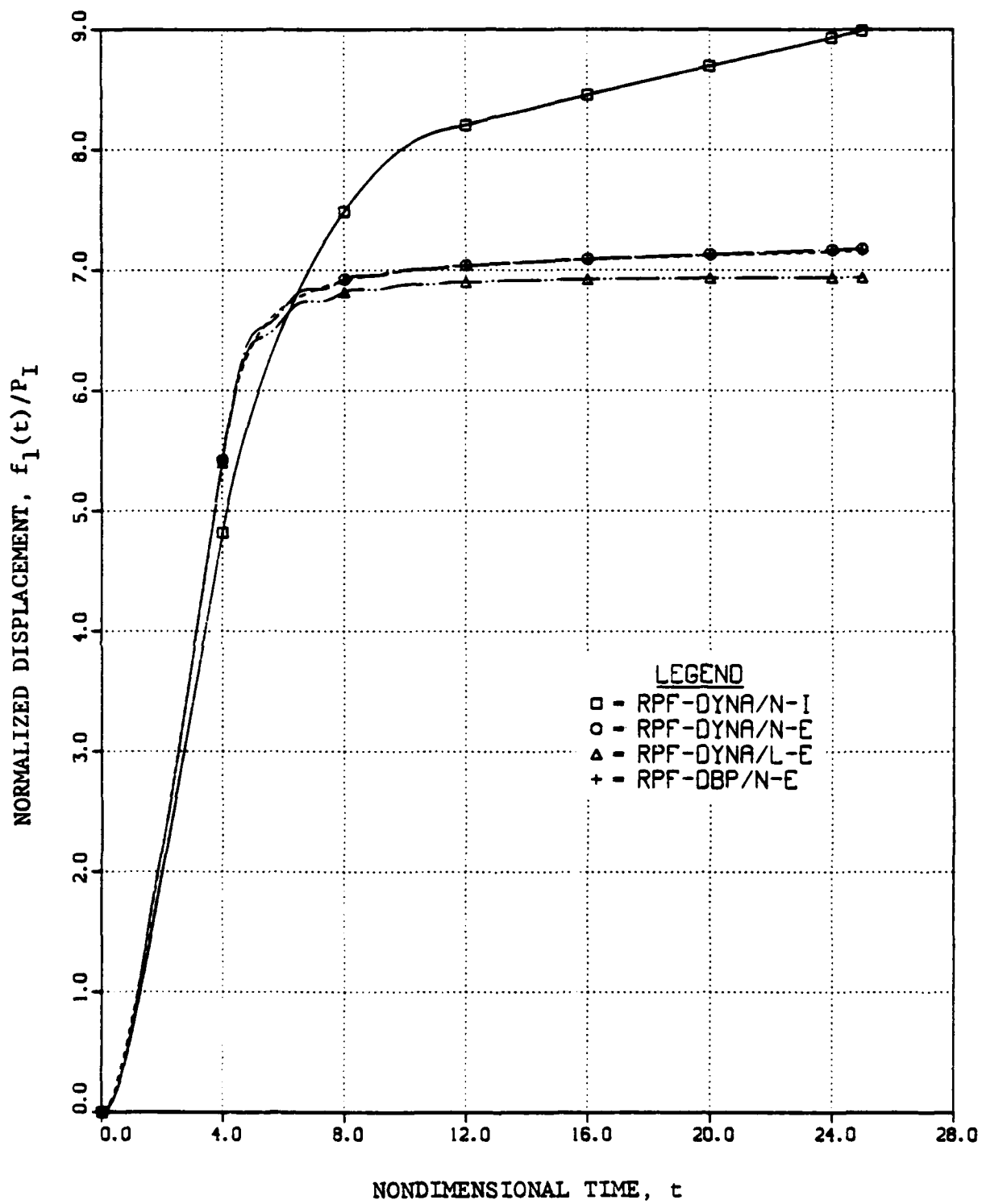


Figure 3.  $n=1$  Rigid-Body Displacement Response of Compromise Shell  
 $(P_I = 4P_c \approx 4P_o, T_I = 4)$

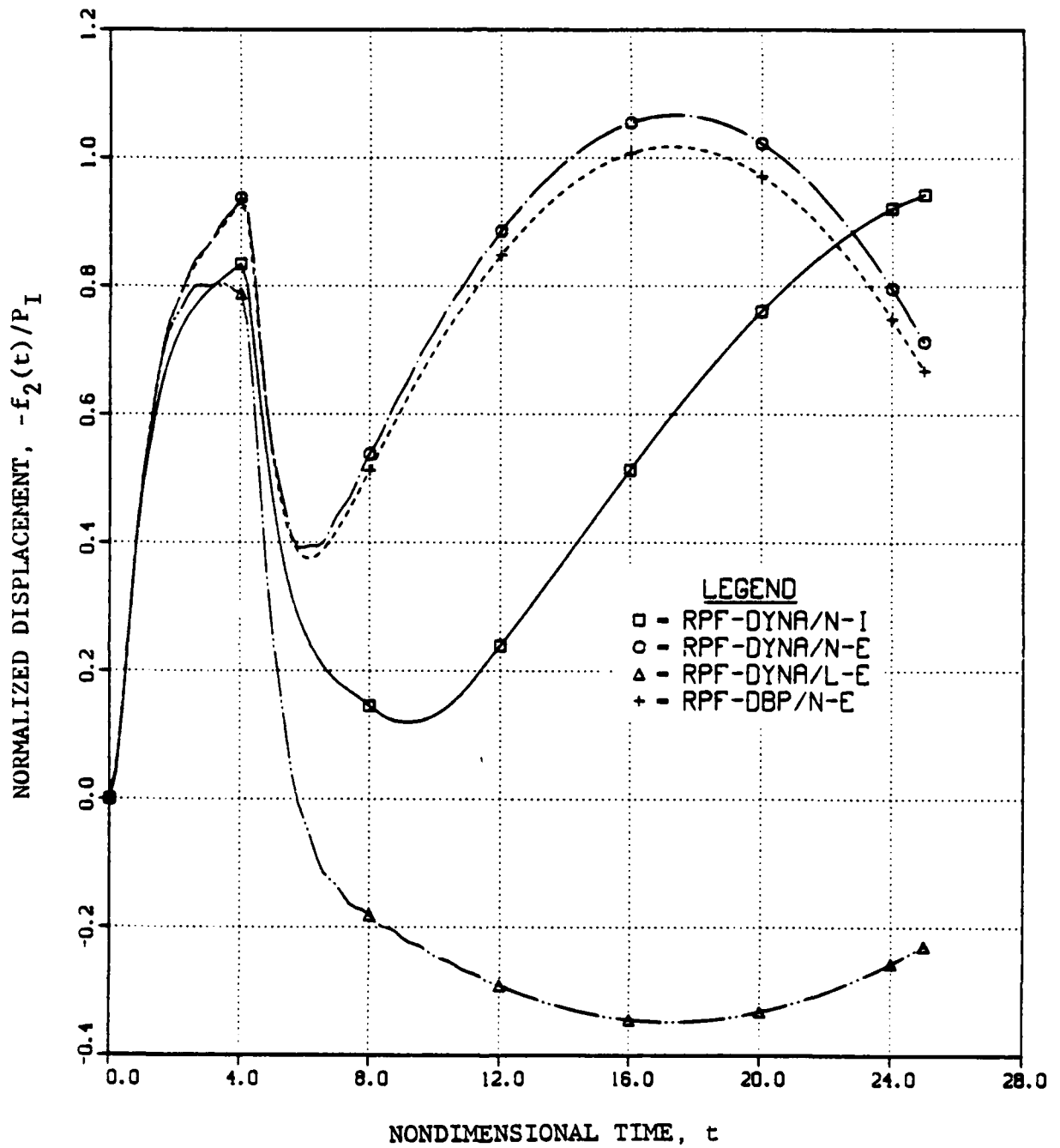


Figure 4.  $n=2$  Flexural Displacement Response of Compromise Shell  
 $(P_I = 4P_c \approx 4P_o, T_I = 4)$

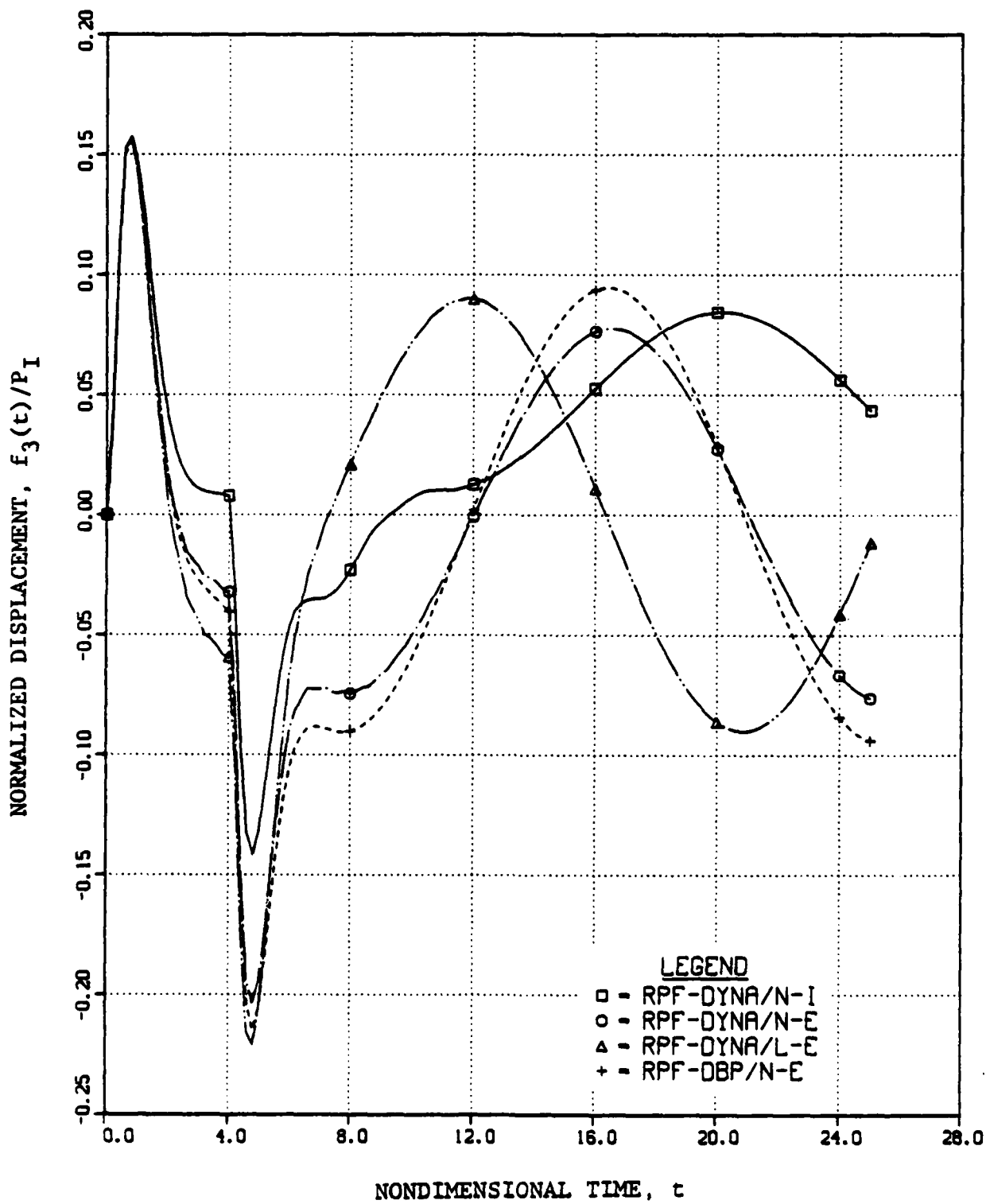


Figure 5.  $n=3$  Flexural Displacement Response of Compromise Shell  
 $(P_I = 4P_C = 4P_O, T_I = 4)$

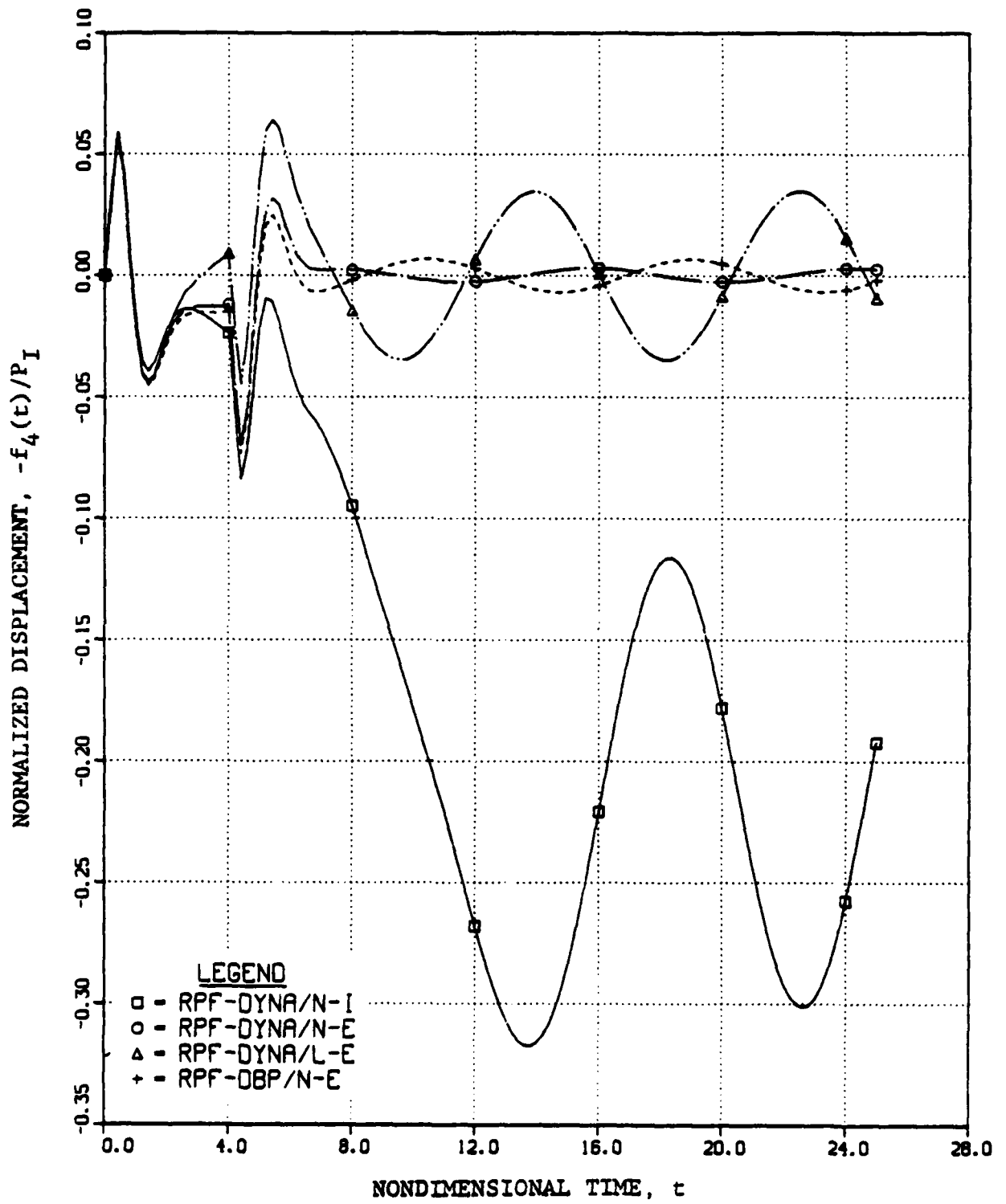


Figure 6.  $n=4$  Flexural Displacement Response of Compromise Shell  
 $(P_I = 4P_C = 4P_0, T_I = 4)$

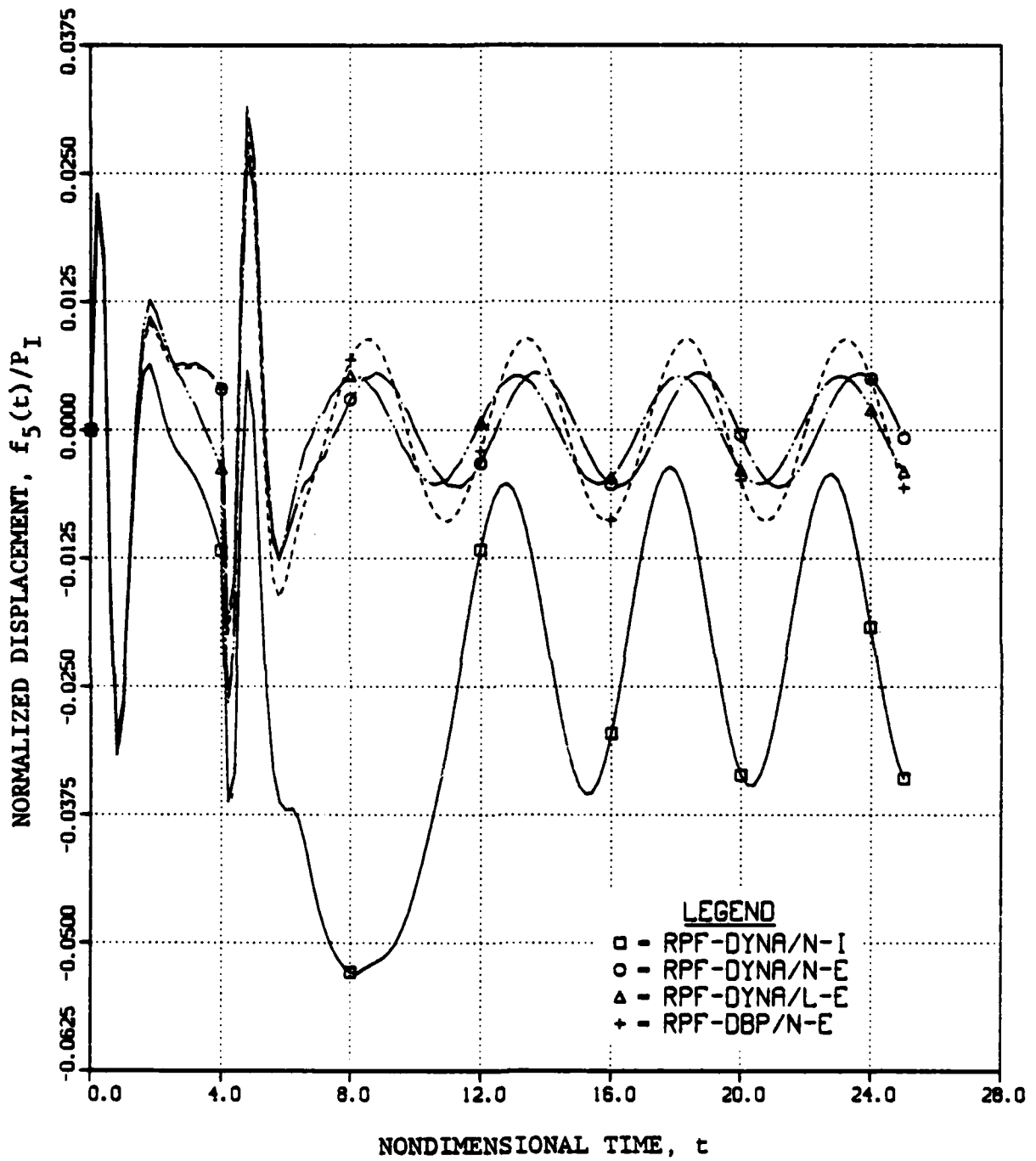


Figure 7.  $n=5$  Flexural Displacement Response of Compromise Shell  
 $(P_I = 4P_c \approx 4P_o, T_I = 4)$

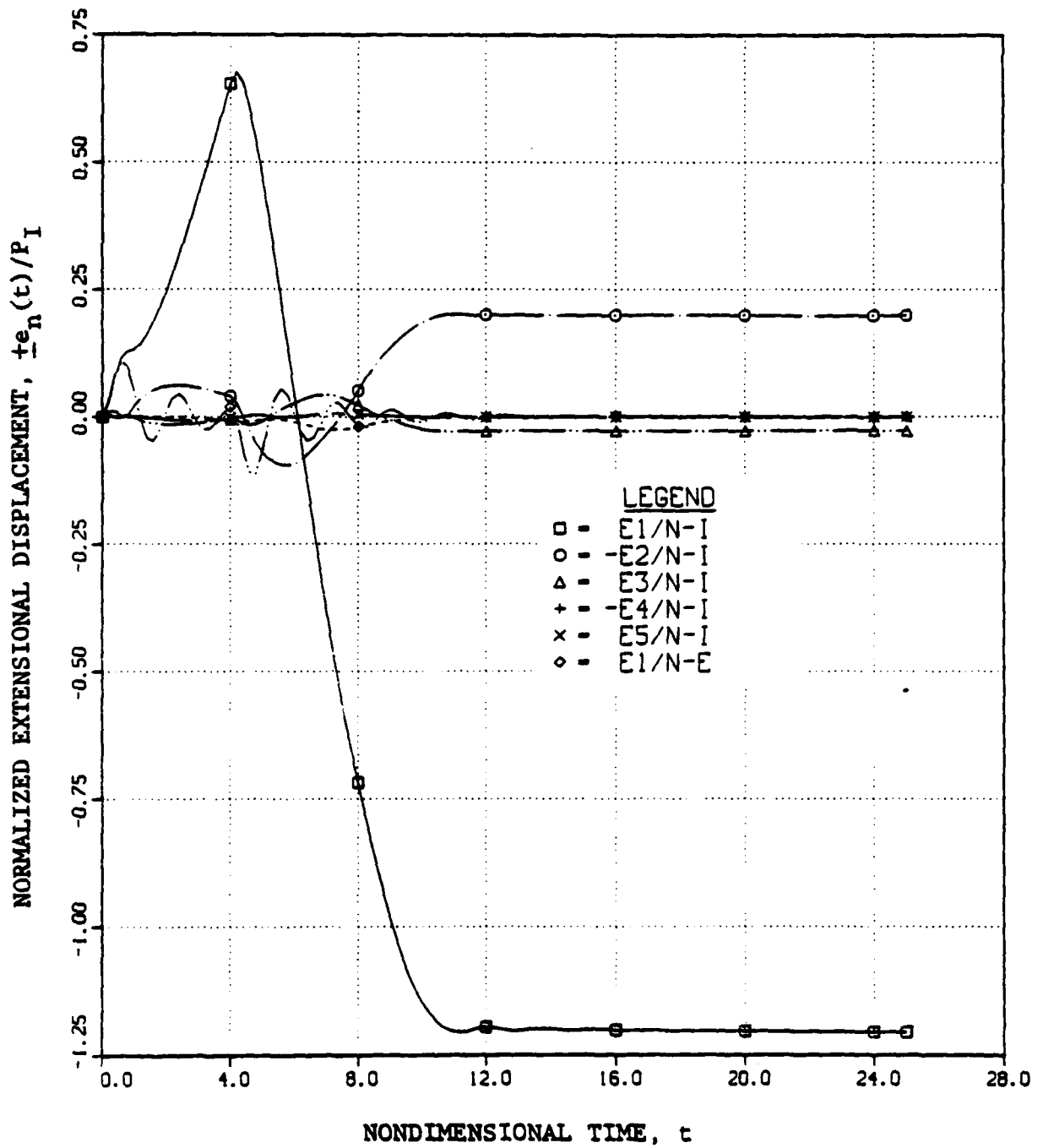


Figure 8. Nonaxisymmetric Extensional Displacement Response of Compromise Shell ( $P_I = 4P_c \approx 4P_o$ ,  $T_I = 4$ )

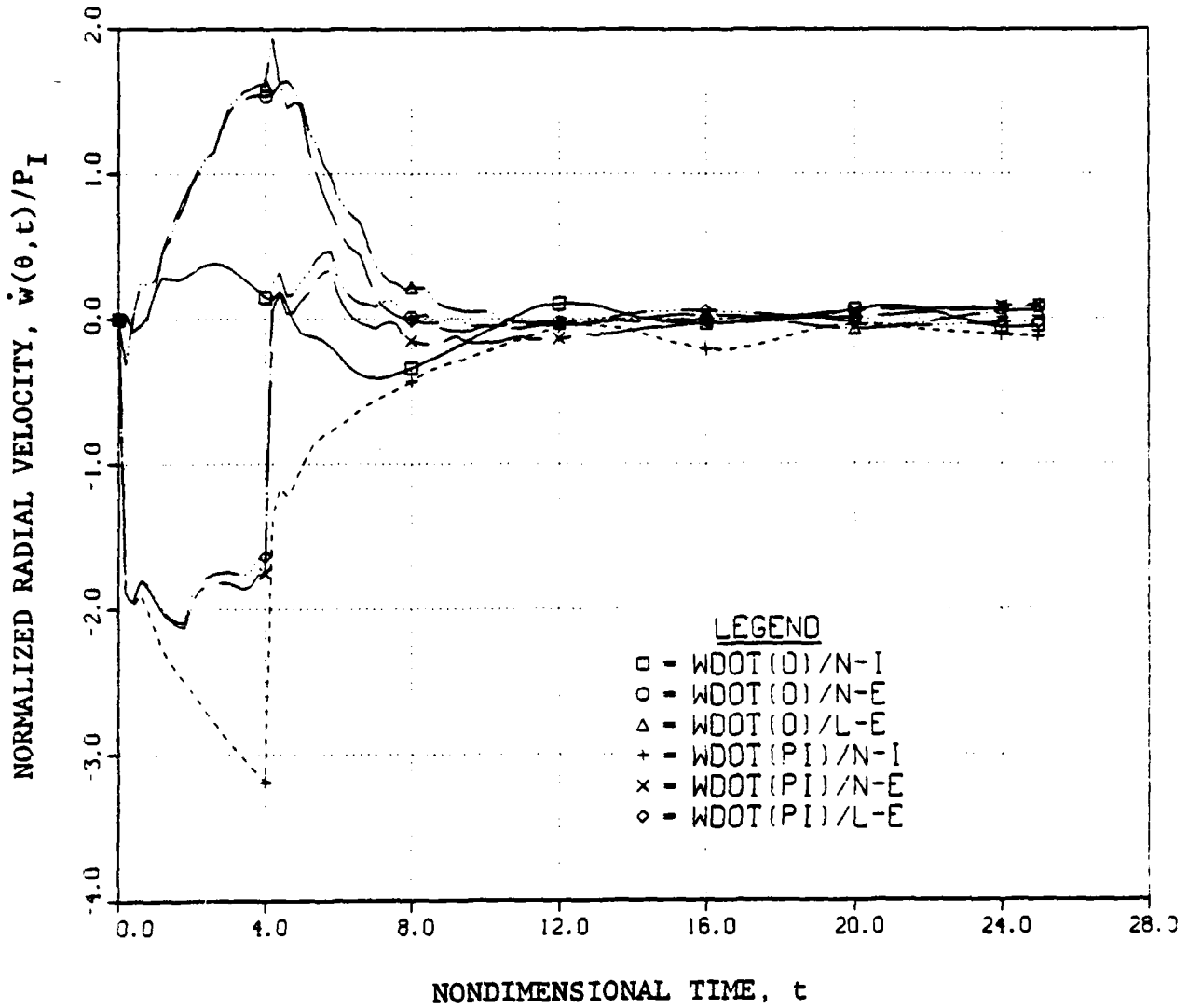


Figure 9. RPF-DYNA Velocity Response of Compromise Shell  
 $(P_I = 4P_c = 4P_o, T_I = 4)$

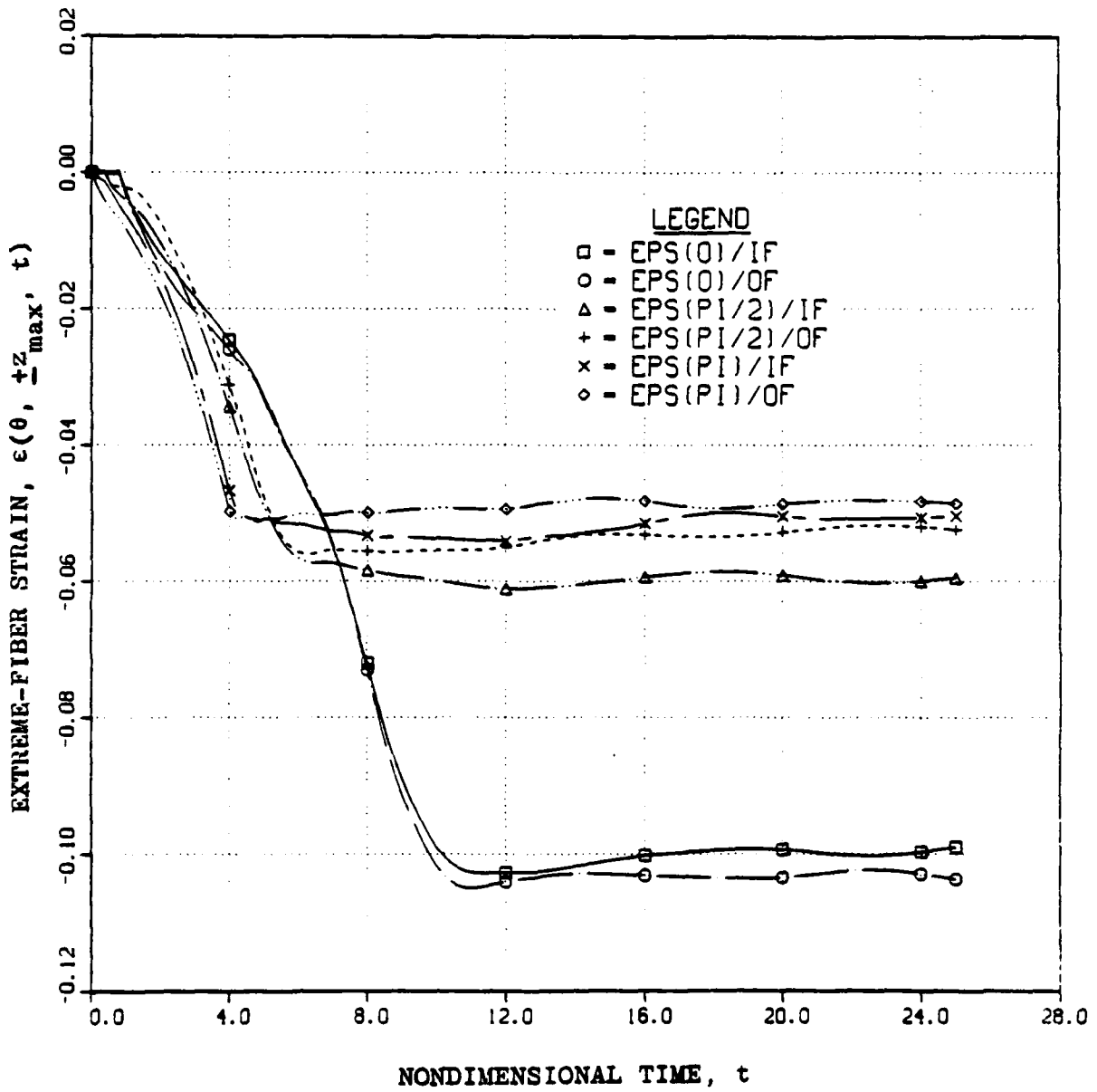
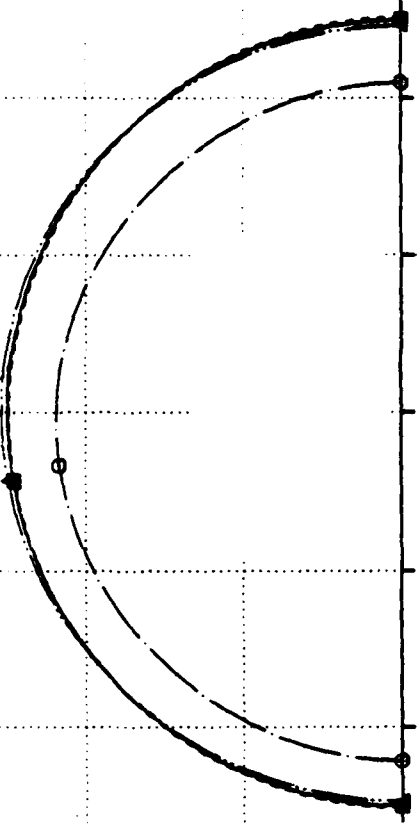
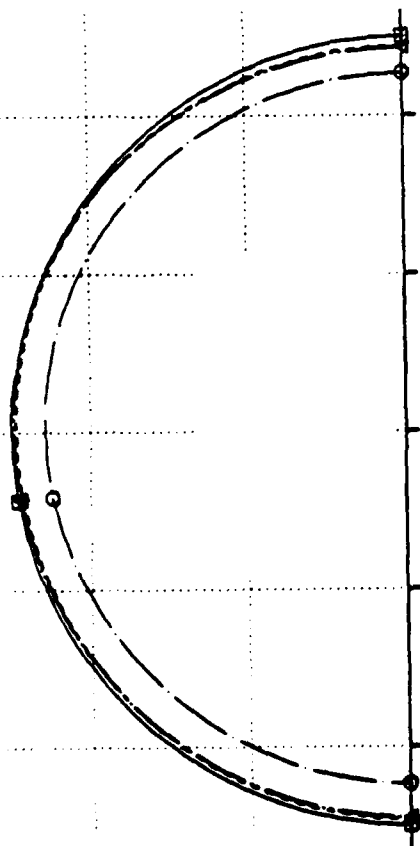


Figure 10. RPF-DYNA Strain Response of Compromise Shell (IF denotes inner fiber; OF denotes outer fiber;  $P_I = 4P_c \approx 4P_o$ ,  $T_I = 4$ )

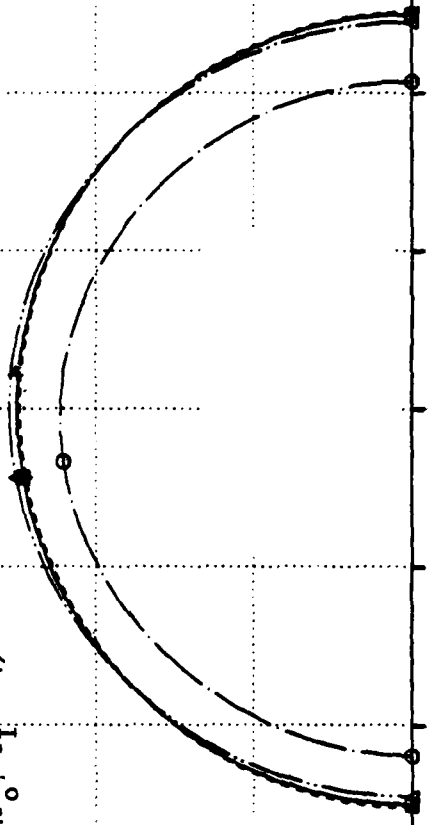
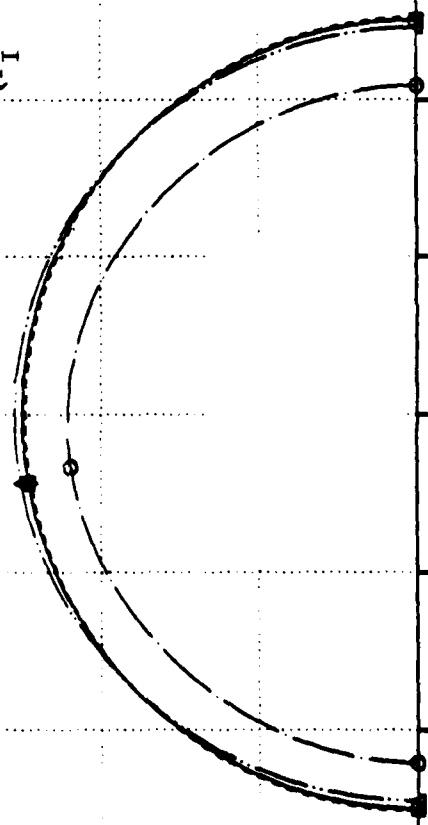


DISPLACEMENT AT T-5

DISPLACEMENT AT T-10

- = UNDEFORMED SHELL
- = INELASTIC RESPONSE
- △ = NONLINEAR-ELASTIC RESPONSE
- + = LINEAR-ELASTIC RESPONSE

$$(P_I = 4P_C \approx 4P_0, T_I = 4)$$



DISPLACEMENT AT T-15

DISPLACEMENT AT T-20

Figure 11. Deformation Snapshots for the Compromise Shell (actual deformations magnified two times)

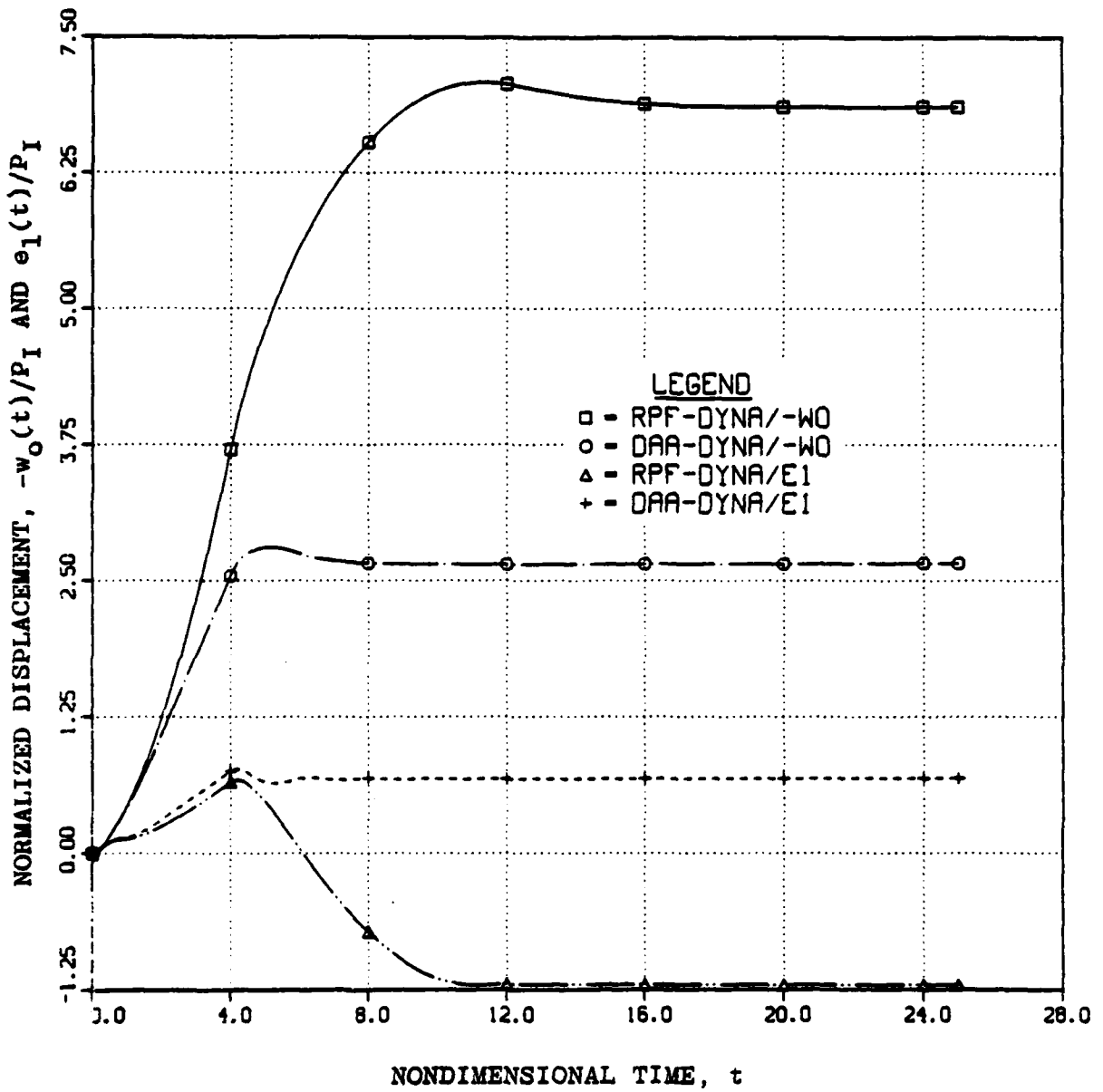


Figure 12.  $n=0$  and  $n=1$  Extensional Displacement Response of Compromise Shell as Computed with RPF-DYNA and DAA-DYNA ( $P_I = 4P_c = 4P_o$ ,  $T_I = 4$ )

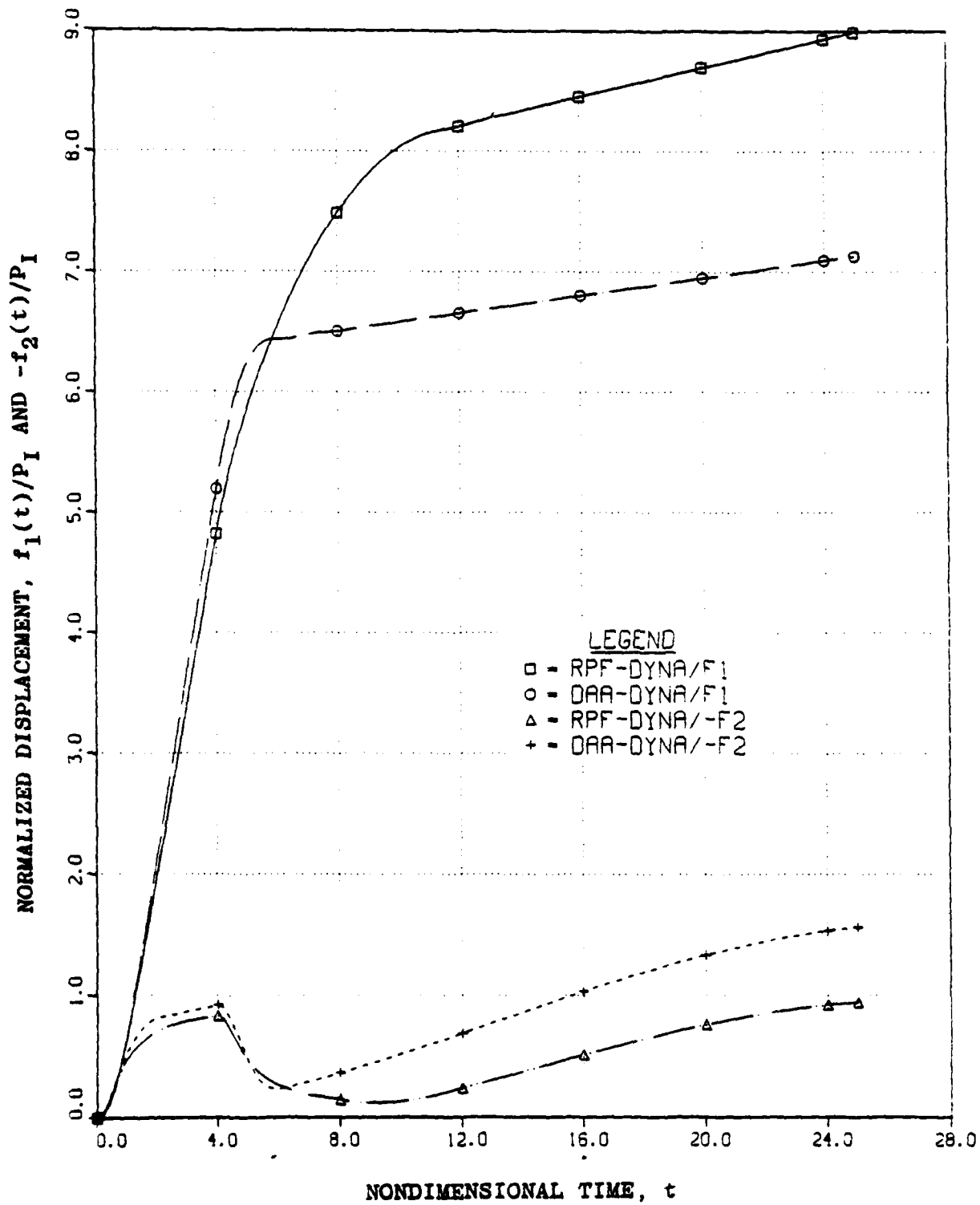


Figure 13. n=1 and n=2 Flexural Displacement Response of Compromise Shell as Computed with RPF-DYNA and DAA-DYNA ( $P_I = 4P_C = 4P_0$ ,  $T_I = 4$ )

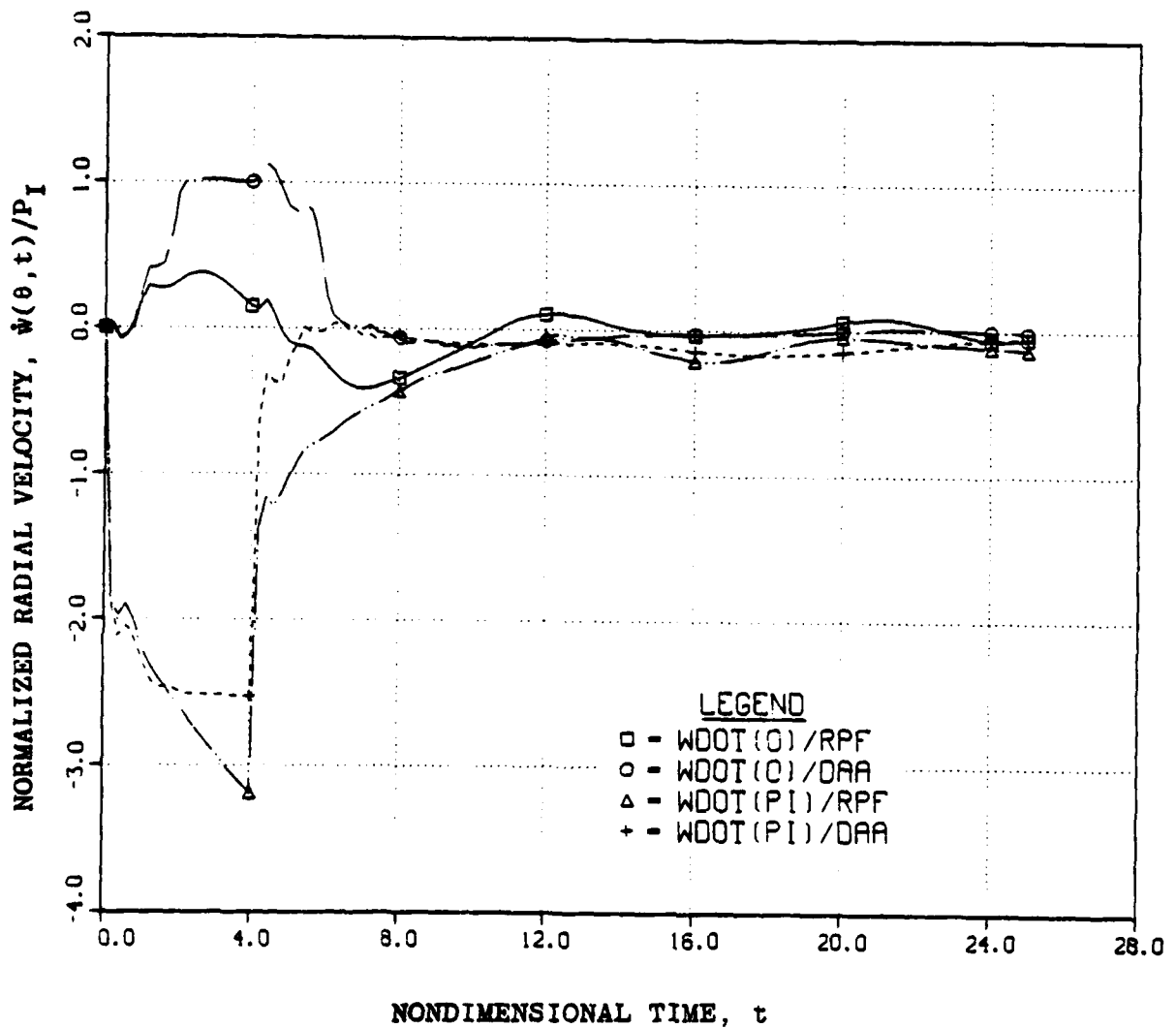


Figure 14. Velocity Response of Compromise Shell as Computed with RPF-DYNA and DAA-DYNA ( $P_I = 4P_C \cong 4P_O$ ,  $T_I = 4$ )

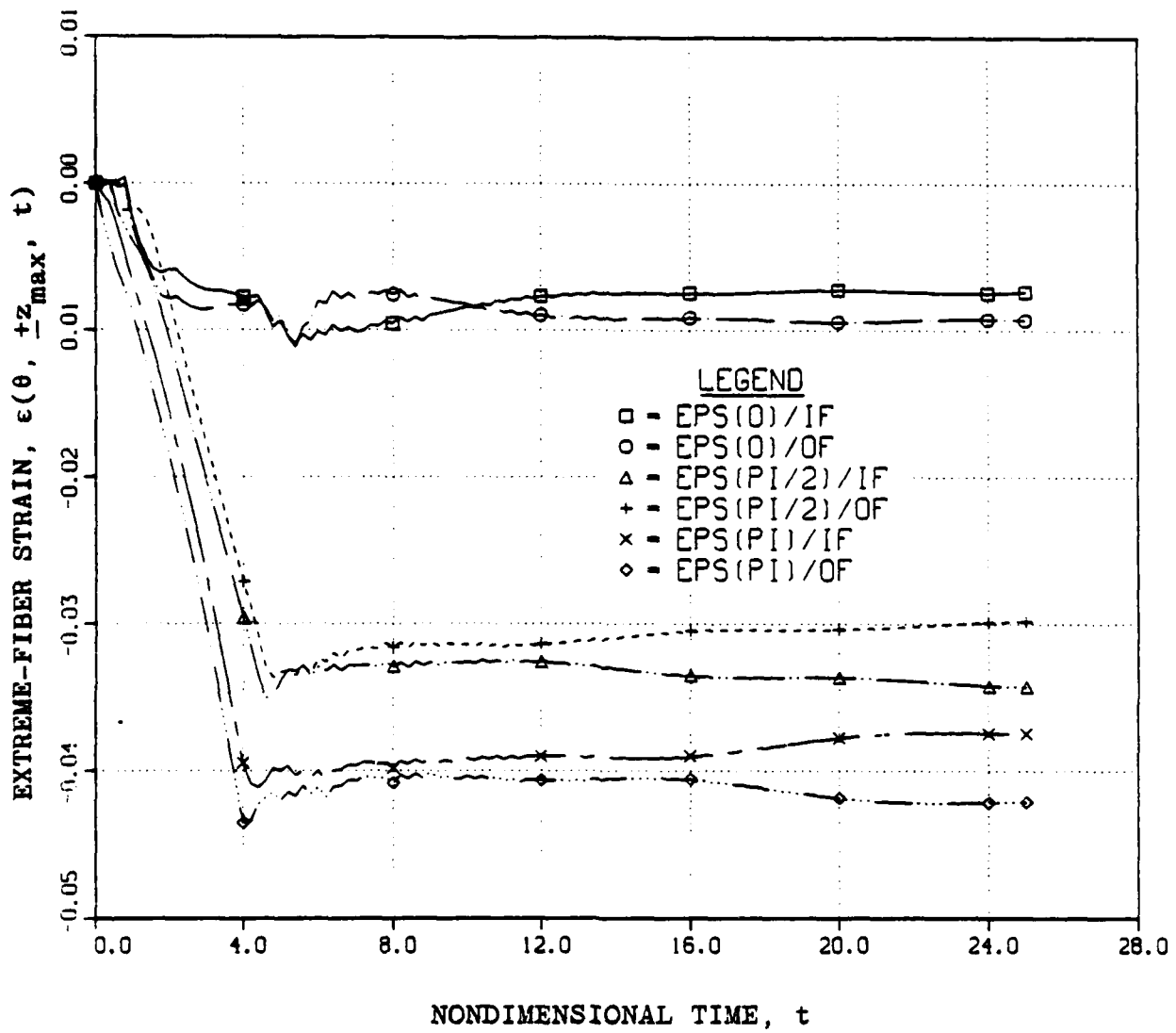


Figure 15. DAA-DYNA Strain Response of Compromise Shell (IF denotes inner fiber; OF denotes outer fiber;  $P_I = 4P_c = 4P_o$ ,  $T_I = 4$ )

Appendix

REMOVAL OF RIGID-BODY SHELL MOTION

The deformation snapshots of Figure 11 have been produced through the omission of rigid-body shell motion during Fourier superposition of the shell response harmonics. Such motion is given by  $v(\theta, t) = -f_1(t) \sin\theta$ ,  $w(\theta, t) = f_1(t) \cos\theta$ , where  $f_1(t)$  is defined in (16). Now (16) may be inverted to yield

$$e_n = \frac{n}{n^2+1} (v_n + \frac{1}{n} w_n) \tag{18}$$

$$f_n = \frac{n}{n^2+1} (-v_n + n w_n)$$

The omission of  $f_n$  from (16) then yields

$$v_n^* = \frac{n^2}{n^2+1} (v_n + \frac{1}{n} w_n) \tag{19}$$

$$w_n^* = \frac{n}{n^2+1} (v_n + \frac{1}{n} w_n)$$

which, for  $n = 1$ , lead to the coefficients of  $\sin\theta$  and  $\cos\theta$  in (17).

DISTRIBUTION

Assistant to the Secretary of Defense  
Atomic Energy  
Washington, DC 20301  
Attn: Executive Assistant

Director  
Defense Advanced Research Project Agency  
1400 Wilson Blvd.  
Arlington, VA 22209  
Attn: TIO

Defense Documentation Center  
Cameron Station  
Alexandria, VA 22314  
Attn: DD

Director  
Defense Intelligence Agency  
Washington, DC 20301  
Attn: RDS-3A (Technical Library)  
DT-2  
DT-1C  
DB-4C

Director  
Defense Nuclear Agency  
Washington, DC 20305  
Attn: DDST  
TITL  
SPSS

Commander  
Field Command  
Defense Nuclear Agency  
Kirtland Air Force Base  
Albuquerque, NM 87115

Chief  
Field Command  
Defense Nuclear Agency  
Livermore Division  
P.O. Box 808, L-317  
Livermore, CA 94550  
Attn: FCPRL

Director  
Interservice Nuclear Weapons School  
Kirtland Air Force Base  
Albuquerque, NM 87115  
Attn: TTV

Director  
Joint Strategic Target Planning Staff  
Offutt Air Force Base  
Omaha, NB 68113  
Attn: NRI-STINFO Library  
JLW/Thompson

Under Secretary of Defense for  
Research and Engineering  
Department of Defense  
Washington, DC 20301  
Attn: Strategic and Space Systems (OS)

Deputy Chief of Staff for Research  
Development and Acquisition  
Department of the Army  
Washington, DC 20310  
Attn: DAMA-CSS-N

Commander  
Harry Diamond Laboratories  
Department of the Army  
2800 Powder Mill Road  
Adelphi, MD 20783  
Attn: DELHD-I-TL (Technical Library)

Director  
U.S. Army Ballistic Research Laboratories  
Aberdeen Proving Ground, MD 21005  
Attn: DRDAR-TSB-S (Technical Labrary)

Director  
U.S. Army Engineering Waterways  
Experimental Station  
P.O. Box 631  
Vicksburg, MS 39180  
Attn: J. Strange  
W. Flathau  
Technical Information Center

Commander  
U.S. Army Material and  
Mechanics Research Center  
Watertown, MA 02172  
Attn: DRXMR-TE, R. Shea

Commander  
U.S. Army Nuclear and  
Chemical Agency  
7500 Backlick Road, Bldg. 2073  
Springfield, VA 22150  
Attn: Library

Commander  
David Taylor Naval Ship  
Research and Development Center  
Bethesda, MD 20084  
Attn: Code 174           1740.6  
                  1740.4   L42-3 (Library)  
                  1740.1   11  
                  173       1740.5  
                  1844     172  
                  1770.1   2740

Officer in Charge  
Naval Construction Battalion Center  
Civil Engineering Laboratory  
Port Hueneme, CA 93041  
Attn: Code L08A (Library)

Commander  
Naval Electronic Systems Command  
Washington, DC 20360  
Attn: PME 117-21

Commander  
Naval Facilities Engineering Command  
Washington, DC 20390  
Attn: Code 09M22C (Technical Library)

Headquarters  
Naval Material Command  
Washington, DC 20360  
Attn: MAT 08T-22

Commander  
Naval Ocean Systems Center  
San Diego, CA 92152  
Attn: Code 4471 (Technical Library)

Superintendent  
Naval Postgraduate School  
Monterey, CA 93940  
Attn: Code 0142 (Library)  
69NE

Commander  
Naval Sea Systems Command  
Washington, DC 20362  
Attn: SEA 08  
          SEA 322  
          SEA 09G53 (Library)  
          SEA 323  
          SEA 3221

Commanding Officer  
Naval Research Laboratory  
Washington, DC 20375  
Attn: Code 8100  
          8440  
          8003  
          8301  
          6380  
          2627 (Technical Library)  
          8445

Officer in Charge  
Naval Surface Weapons Center  
White Oak Laboratory  
Silver Spring, MD 20910  
Attn: Code R14  
          R13  
          F31  
          R10  
          R15

Commander  
Naval Surface Weapons Center  
Dahlgren, VA 22448  
Attn: Technical Library and  
Information Services Branch

Commander  
Naval Weapons Center  
China Lake, CA 93555  
Attn: Code 233 (Technical Library)

Commanding Officer  
Naval Weapons Evaluation Facility  
Kirtland Air Force Base  
Albuquerque, NM 87117  
Attn: Code 210  
          10 (Technical Library)  
          G. Binns

Commanding Officer  
NWSC Crane  
Crane, IN 47401  
Attn: Code 70553

Officer in Charge  
New London Laboratory  
Naval Underwater Systems Center  
New London, CT 06320  
Attn: Code 401, J. Kalinowski  
          401, J. Patel

Officer in Charge  
Newport Laboratory  
Naval Underwater Systems Center  
Newport, RI 02840  
Attn: Code EM  
363, P. Paranzino

Office of Naval Research  
Arlington, VA 22217  
Attn: Code 474, N. Perrone

Office of the Chief of Naval Operations  
Washington, DC 20350  
Attn: OP 981  
OP 982 OP 37  
OP 953 OP 604C  
OP 981N1 OP 03EG  
OP 957E OP 987  
OP 951 OP 21

Director  
Strategic Systems Project Office  
Department of the Navy  
Washington, DC 20376  
Attn: NSP-272  
NSP-43 (Technical Library)

Air Force Institute of Technology  
Air University  
Wright-Patterson Air Force Base  
Dayton, OH 45433  
Attn: Library

Air Force Weapons Laboratory, AFSC  
Kirtland Air Force Base  
Albuquerque, NM 87117  
Attn: SUL

Bolt Beranek & Newman, Inc.  
Union Station  
New London, CT 06320  
Attn: R. Haberman

Cambridge Acoustical Associates, Inc.  
54 Rindge Avenue Extension  
Cambridge, MA 02140  
Attn: M. Junger

Columbia University  
Department of Civil Engineering  
S. W. Mudd Building  
New York, NY 10027  
Attn: F. DiMaggio

General Dynamics Corporation  
Electric Boat Division  
Eastern Point Road  
Groton, CT 06340  
Attn: M. Pakstys

General Electric Co.  
816 State Street  
P.O. Drawer QQ  
Santa Barbara, CA 93102  
Attn: DASIAC

Kaman Sciences Corp.  
P.O. Box 7463  
Colorado Springs, CO 80933  
Attn: Library

Merritt Cases, Inc.  
P.O. Box 1206  
Redlands, CA 92373  
Attn: Library

Pacifica Technology  
P.O. Box 148  
Del Mar, CA 92014  
Attn: J. Kent

Patel Enterprises, Inc.  
2907 Governors Drive  
Huntsville, AL 35805  
Attn: M. Patel

Physics Applications, Inc.  
828 Charcot Avenue  
San Jose, CA 95131  
Attn: C. Vincent

SRI International  
333 Ravenswood Avenue  
Menlo Park, CA 94025  
Attn: G. Abrahamson  
A. Florence

Tetra Tech, Inc.  
630 N. Rosemead Boulevard  
Pasadena, CA 91107  
Attn: Library (Unclassified Only)  
L. Hwang (Unclassified Only)

Weidlinger Associates Consulting  
Engineers  
110 East 59th Street  
New York, NY 10022  
Attn: M. Baron

Weidlinger Associates Consulting  
Engineers  
3000 Sand Hill Road  
Menlo Park, CA 94025  
Attn: J. Isenberg

UNCLASSIFIED

SECURITY CLASSIFICATION OF THIS PAGE (When Data Entered)

REPORT DOCUMENTATION PAGE		READ INSTRUCTIONS BEFORE COMPLETING FORM
1. REPORT NUMBER 14 LMSC/D676214	2. GOVT ACCESSION NO. AD-A088597	3. RECIPIENT'S CATALOG NUMBER
4. TITLE (and Subtitle) 6 INELASTIC RESPONSE OF AN INFINITE CYLINDRICAL SHELL TO A TRANSIENT ACOUSTIC WAVE.	5. DATE OF REPORT & PERIOD COVERED 9 Final Report for Period 1 August 1977-31 March 1979	6. PERFORMING ORG. REPORT NUMBER LMSC-D676214
7. AUTHOR(s) 10 T. L. Geers C.-L. Yen	8. CONTRACT OR GRANT NUMBER(s) 15 N00014-77-C-0562/reu	
9. PERFORMING ORGANIZATION NAME AND ADDRESS Lockheed Palo Alto Research Laboratory 3251 Hanover Street, Palo Alto, CA 94304	10. PROGRAM ELEMENT, PROJECT, TASK AREA & WORK UNIT NUMBERS 16 61153N 17 RR02303 RR0230301/	
11. CONTROLLING OFFICE NAME AND ADDRESS Office of Naval Research 800 N. Quincy St. Arlington, VA 22217	12. REPORT DATE 11 March 1979	
14. MONITORING AGENCY NAME & ADDRESS (if different from Controlling Office) 19421	13. NUMBER OF PAGES 35	15. SECURITY CLASS. (of this report) UNCLASSIFIED
	15a. DECLASSIFICATION/DOWNGRADING SCHEDULE	
16. DISTRIBUTION STATEMENT (of this Report) Approved for public release; distribution unlimited.		
17. DISTRIBUTION STATEMENT (of the abstract entered in Block 20, if different from Report)		
18. SUPPLEMENTARY NOTES		
19. KEY WORDS (Continue on reverse side if necessary and identify by block number) Fluid-Structure Interaction Inelastic Behavior Transient Shell Response		
20. ABSTRACT (Continue on reverse side if necessary and identify by block number) An analytical/computational technique has been developed for determining the geometrically and constitutively nonlinear response of an infinite cylindrical shell to a transverse, transient acoustic wave. Shell behavior has been treated through utilization of the nonlinear structural analyzer DYNAPLAS II, while the fluid-structure interaction has been treated with both the exact residual potential formulation and the doubly asymptotic approximation. Numerical results produced through application of the approximation differ significantly from the corresponding exact results.		

UNCLASSIFIED

SECURITY CLASSIFICATION OF THIS PAGE (When Data Entered)

210118

Handwritten initials/signature